

Graph Wave Networks

Juwei Yue*

Institute of Information Engineering,
Chinese Academy of Sciences
School of Cyber Security, UCAS[†]
Beijing, China
yuejuwei@iie.ac.cn

Haikuo Li*

Institute of Information Engineering,
Chinese Academy of Sciences
School of Cyber Security, UCAS
Beijing, China
lihaikuo@iie.ac.cn

Jiawei Sheng[†]

Institute of Information Engineering,
Chinese Academy of Sciences
Beijing, China
shengjiawei@iie.ac.cn

Yihan Guo

Institute of Information Engineering,
Chinese Academy of Sciences
School of Cyber Security, UCAS
Beijing, China
guoyihan@iie.ac.cn

Xinghua Zhang

Tongyi Lab, Alibaba Group
Beijing, China
zxh.zhangxinghua@gmail.com

Chuan Zhou

Academy of Mathematics and
Systems Science,
Chinese Academy of Sciences
School of Cyber Security, UCAS
Beijing, China
zhouchuan@amss.ac.cn

Tingwen Liu[†]

Institute of Information Engineering,
Chinese Academy of Sciences
School of Cyber Security, UCAS
Beijing, China
liutingwen@iie.ac.cn

Li Guo

Institute of Information Engineering,
Chinese Academy of Sciences
School of Cyber Security, UCAS
Beijing, China
guoli@iie.ac.cn

Abstract

Dynamics modeling has been introduced as a novel paradigm in message passing (MP) of graph neural networks (GNNs). Existing methods consider MP between nodes as a *heat diffusion* process, and leverage *heat equation* to model the temporal evolution of nodes in the embedding space. However, heat equation can hardly depict the wave nature of graph signals in graph signal processing. Besides, heat equation is essentially a partial differential equation (PDE) involving a first partial derivative of time, whose numerical solution usually has low stability, and leads to inefficient model training. In this paper, we would like to depict more wave details in MP, since graph signals are essentially wave signals that can be seen as a superposition of a series of waves in the form of eigenvector. This motivates us to consider MP as a *wave propagation process* to capture the temporal evolution of wave signals in the space. Based on *wave equation* in physics, we innovatively develop a *graph wave equation* to leverage the wave propagation on graphs. In details, we demonstrate that the graph wave equation can be connected

to traditional spectral GNNs, facilitating the design of *graph wave networks (GWNs)* based on various Laplacians and enhancing the performance of the spectral GNNs. Besides, the graph wave equation is particularly a PDE involving a second partial derivative of time, which has stronger stability on graphs than the heat equation that involves a first partial derivative of time. Additionally, we theoretically prove that the numerical solution derived from the graph wave equation are *constantly stable*, enabling to significantly enhance model efficiency while ensuring its performance. Extensive experiments show that GWNs achieve state-of-the-art and efficient performance on benchmark datasets, and exhibit outstanding performance in addressing challenging graph problems, such as over-smoothing and heterophily. Our code is available at <https://github.com/YueAWu/Graph-Wave-Networks>.

CCS Concepts

• **Computing methodologies** → **Neural networks**.

Keywords

Graph Neural Networks, Partial Differential Equations, Wave Equation

ACM Reference Format:

Juwei Yue, Haikuo Li, Jiawei Sheng, Yihan Guo, Xinghua Zhang, Chuan Zhou, Tingwen Liu, and Li Guo. 2025. Graph Wave Networks. In *Proceedings of the ACM Web Conference 2025 (WWW '25)*, April 28–May 2, 2025, Sydney, NSW, Australia. ACM, New York, NY, USA, 15 pages. <https://doi.org/10.1145/3696410.3714673>

*Equal contribution

[†]Corresponding authors

[‡]University of Chinese Academy of Sciences

Permission to make digital or hard copies of all or part of this work for personal or classroom use is granted without fee provided that copies are not made or distributed for profit or commercial advantage and that copies bear this notice and the full citation on the first page. Copyrights for components of this work owned by others than the author(s) must be honored. Abstracting with credit is permitted. To copy otherwise, or republish, to post on servers or to redistribute to lists, requires prior specific permission and/or a fee. Request permissions from permissions@acm.org.
WWW '25, Sydney, NSW, Australia

© 2025 Copyright held by the owner/author(s). Publication rights licensed to ACM.
ACM ISBN 979-8-4007-1274-6/2025/04
<https://doi.org/10.1145/3696410.3714673>

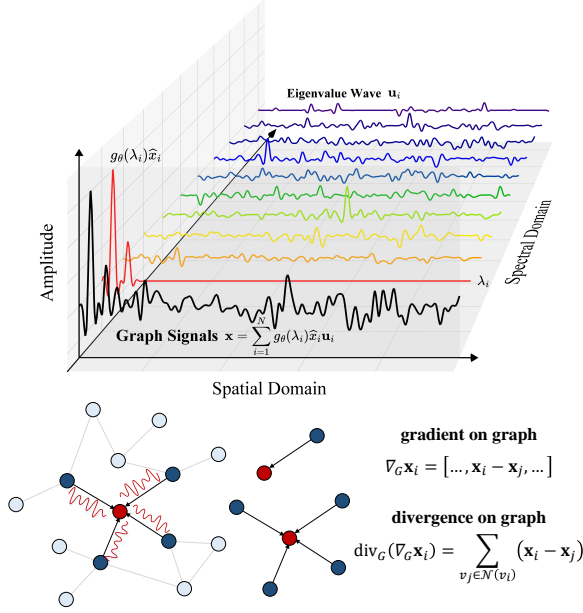


Figure 1: Top: the partial spectrum on the real-world dataset Cora, where the graph signal can be treated as a superposition of multiple eigenvector waves u_i with amplitude $g_\theta(\lambda_i)\hat{x}_i$ (detailed in Eq. (7)). Bottom: the mechanism of wave propagation on the graph (detailed in Sec. 3.2).

1 Introduction

The widespread availability of graph data has propelled the development of *graph neural networks* (GNNs) [48]. These methods have achieved significant success in various applications, such as recommender systems [47], social network analysis [27], particle physics [38], and drug discovery [13].

Currently, mainstream GNNs [10, 20] develop *message passing* (MP) paradigm with graph signal processing [39], which delivers messages node-by-node by stacking graph convolutional layers. In fact, the MP paradigm can be modelled as a differential equation [6]. Recent studies explore *partial differential equations* (PDEs) [6, 24, 42] to consider the spatial and temporal relationships in MP. Intuitively, they analogize MP to a *heat diffusion* process between nodes, and thus leverage the heat equation to model nodes in the embedding space. In physics, the heat equation describes the evolution of temperature in the space over time. Consider 3-dimension spatial variables $(\omega_1, \omega_2, \omega_3)$ in the space and a time variable t , the **Heat Equation** is:

$$\frac{\partial u}{\partial t} = \alpha \left(\frac{\partial^2 u}{\partial \omega_1^2} + \frac{\partial^2 u}{\partial \omega_2^2} + \frac{\partial^2 u}{\partial \omega_3^2} \right) = \alpha \cdot \text{div}(\nabla u), \quad (1)$$

where u is the abbreviation symbol for $u(\omega_1, \omega_2, \omega_3, t)$, denoting the temperature at position $(\omega_1, \omega_2, \omega_3)$ and time t , and α is a coefficient called the thermal diffusivity of the medium. However, in context of graph learning, these methods suffer from two drawbacks: *First, the heat equation can hardly depict the wave nature of graph signals.* In graph signal processing theory [39], the graph can be seen as a combination of waves with different frequencies, where we show

Table 1: Graph heat equation and graph wave equation. $X = X(t)$, ∇ and div denote gradient and divergence.

Graph Heat Equation	$\frac{\partial X}{\partial t} = \text{div}[\text{diag}(a(x_i, x_j)) \nabla X], X \in \mathbb{R}^{N \times d}$	
	$(\nabla X)_{ij} = x_j - x_i$	$\text{div}[\nabla X]_i = \sum_{v_j \in N(v_i)} (x_j - x_i)$
Graph Wave Equation	$\frac{\partial X}{\partial t} = a^2[\dots, \text{div}_G((\nabla_G X)_i), \dots]^T, X \in \mathbb{R}^{N \times d}$	
	$\nabla_G X_i = [\dots, x_i - x_j, \dots]$	$\text{div}_G(\nabla_G X_i) = \sum_{v_j \in N(v_i)} (x_i - x_j)$

the graph wave spectrum in Figure 1 (Top). The heat equation is naturally not capable to process the details of wave property in message passing, which leads to coarse and sub-optimal GNN designs. *Second, the heat equation is essentially a PDE involving a first partial derivative of time, yet its stability of numerical solution can be poor on graph.* This requires small time step lengths in solving PDE, leading to low efficiency in model training, and can be easily affected by initial values and generate unsatisfactory performance. We also give the experimental evidence in Sec. 4.

Unlike previous studies [6, 24, 42] that regard MP as a heat diffusion process, we innovatively analogize MP to a *wave propagation* process. Particularly, MP basically embodies the information propagation along the nodes at different spatial positions and temporal steps, which bears a strong resemblance to the propagation of *waves* in physics, such as electromagnetic waves. To depict the wave propagation process, we explore the wave equation, a PDE involving the second derivative of time, which describes the evolution of wave intensity over time and has wide applicability in physics. Also consider the three spatial variables $(\omega_1, \omega_2, \omega_3)$ and a time variable t , the **Wave Equation** is:

$$\frac{\partial^2 u}{\partial t^2} = a^2 \left(\frac{\partial^2 u}{\partial \omega_1^2} + \frac{\partial^2 u}{\partial \omega_2^2} + \frac{\partial^2 u}{\partial \omega_3^2} \right) = a^2 \cdot \text{div}(\nabla u), \quad (2)$$

where u is the abbreviation symbol for $u(\omega_1, \omega_2, \omega_3, t)$, denoting the wave intensity at position $(\omega_1, \omega_2, \omega_3)$ and time t , and a is a coefficient denoting the propagation speed of the wave. Notably, though the wave equation has similar formulation as heat equation, it has intrinsically different properties in the context of graph learning: *First, wave equation is naturally suitable for MP in GNNs.* Since GNN is actually a wave filter of frequencies, it can be achieved by Laplacian. It investigates more details in processing graph signals, offering higher accuracy and practicality compared to heat equation. *Second, the wave equation is essentially a PDE involving a second partial derivative of time, which can offer stronger stable condition on graph.* This property provides more efficient training process that allows larger time step lengths, and often generates robust experimental results (see Figure 4). The wave propagation process on graph can be depicted as Figure 1 (Bottom).

Though applying the above wave equation to MP is attractive and reasonable, the specific MP formulation of wave equation is not obvious, and it is non-trivial to conduct further exploration. To this end, our breakthrough point is to *formulate the MP process with the wave equation at each node*, since once the MP process is specified, the overall GNN is designed. Therefore, we first would like to derive

graph wave equation for MP. Inspired by Chamberlain et al. [6], we let the gradient on graph be the difference of features between a central node and each of its neighbors, and the divergence be the total difference of them. Thereby we can derive the formulation in *graph wave equation*, and the details are shown in Table 1. By introducing the characteristics of graph Laplacian, the graph wave equation can be further rewritten into a brief form for the solution of PDEs (detailed in Sec. 3.2).

Based upon the above derived graph wave equation, we then would like to achieve the MP for GNN design by solving PDEs. In fact, the solution of PDEs is often an iterative node feature update process, which can actually be interpreted as the MP process. Existing PDE-based GNN methods [6, 30] utilizing the *forward Euler method* to solve PDEs, resulting in conditionally stable *explicit schemes*, making it difficult to balance the performance and efficiency of the model. Besides, Chamberlain et al. [6] also attempt *implicit schemes* through the *backward Euler method*, which are constantly stable but require solving linear systems, leading to higher computational complexity and lower efficiency compared to the explicit schemes. In this paper, we use the *forward Euler method* to solve the graph wave equation, which can obtain **constantly stable explicit schemes**. This allows the model to significantly improve convergence rates by selecting larger time step lengths, thereby enhancing efficiency of operation while guaranteeing model performance (detailed in Sec. 3.3). Based upon the above designs, we propose the Graph Wave Networks (termed as GWN) with MP formulated by graph wave equation. Two specified implementations are provided to achieve our GWN according to different specifications of Laplacians (detailed in Sec. 3.4).

Our main contributions can be summarized as follows:

- For the first time, we model the message passing from an innovative perspective of a **wave propagation process**, thereby maintaining the wave nature in graph convolutional operation.
- We develop wave equation into **graph wave equation**, and propose a novel **graph wave network**, namely GWN. It establishes a connection between wave equation and traditional spectral GNNs, enhancing them with more details of waves on graphs.
- Through the theoretical evidence, we prove that the explicit scheme of the graph wave equation is **constantly stable**, allowing **significant efficiency improvements** while guaranteeing robust model prediction results.
- We conduct extensive experiments on 9 benchmark datasets. Experimental results substantiate that GWN outperforms previous state-of-the-art methods and achieves efficient performance in alleviating over-smoothing and heterophily.

2 Preliminaries

In this section, we discuss graph signal processing in traditional GNNs, and then introduce fundamental concepts of wave equations.

2.1 Graph Signal Processing

Graph signal processing [39] is a field that focuses on signal analysis and processing conducted on graphs.

Notations of Graph. Given a simple undirected graph \mathcal{G} , composed of a set of nodes \mathcal{V} and a set of edges \mathcal{E} , with $N = |\mathcal{V}|$ nodes in total. Graph \mathcal{G} is associated with a feature matrix $\mathbf{X} \in \mathbb{R}^{N \times d}$,

where the i -th row of \mathbf{X} corresponds to the feature vector $\mathbf{x}_i = [x_{i1}, x_{i2}, \dots, x_{id}] \in \mathbb{R}^d$ of node v_i , and the j -th column of \mathbf{X} corresponds to the graph signal of dimension j . We denote the adjacency matrix as \mathbf{A} and the degree matrix as \mathbf{D} with $D_{ii} = \sum_i A_{ij}$.

Spectral Graph Convolution. Traditional spectral GNNs design spectral graph convolution using the symmetric normalized Laplacian $\mathbf{L}_{sym} = \mathbf{I} - \mathbf{D}^{-1/2} \mathbf{A} \mathbf{D}^{-1/2}$, which can be decomposed into $\mathbf{L}_{sym} = \mathbf{U} \mathbf{\Lambda} \mathbf{U}^T$, where $\mathbf{\Lambda} = \text{diag}(\lambda_1, \lambda_2, \dots, \lambda_N)$ is a diagonal matrix of eigenvalues and \mathbf{U} is a matrix of corresponding eigenvectors. Here, the eigenvalues satisfy $0 = \lambda_1 \leq \dots \leq \lambda_N = 2$. Based on this, the definition of spectral graph convolution is as follows:

$$(\mathbf{g} * \mathbf{X})_G = \mathbf{U} \mathbf{g}_\theta \mathbf{U}^T \mathbf{X}, \quad (3)$$

where $\mathbf{g}_\theta = \mathbf{g}_\theta(\mathbf{\Lambda}) = \text{diag}(g_\theta(\lambda_1), \dots, g_\theta(\lambda_N))$ denotes the graph filter function.

2.2 Wave Equation

The wave equation describes the laws of waves in the space evolving over time, which has been widely adopted to analyze the characteristics of waves like electromagnetic waves in physics.

Given that $u(\omega_1, \dots, \omega_d, t)$ is a scalar-valued function on $\Omega^d \times [0, \infty)$ that reflects the wave intensity, where $\Omega^d = \omega_1 \times \dots \times \omega_d$ denotes the spatial dimension, and $t \in [0, \infty)$ denotes the time dimension, the wave equation can be formulated by the following partial differential equation (PDE):

$$\frac{\partial^2 u}{\partial t^2} = a^2 \left(\frac{\partial^2 u}{\partial \omega_1^2} + \dots + \frac{\partial^2 u}{\partial \omega_d^2} \right) = a^2 \Delta u = a^2 \cdot \text{div}(\nabla u), \quad (4)$$

where $\Delta = \sum_i \frac{\partial^2}{\partial \omega_i^2}$ denotes Laplacian operator in mathematics, ∇ and div denote gradient and divergence, respectively. a denotes the propagation velocity of waves in the medium (such as the propagation velocity of electromagnetic waves in vacuum), which is a scalar or a function to describe the wave.

3 Wave Equation on Graphs

In this section, we would like to analyze the wave nature of graph signals, and propose graph wave equation with solutions for MP.

3.1 Graph and Wave

This section illustrates the connection between graphs and waves from the perspective of graph signal processing. For convenience, we use a toy example of graph signals $\mathbf{x} = [x_1, \dots, x_N]^T \in \mathbb{R}^{1 \times N}$ with N nodes embedded in 1-dimensional space Ω^1 , where the same principle can be extended to d -dimensional space Ω^d . First, the typical implementation of spectral graph convolution transforms graph signals by Fourier transform:

$$\widehat{\mathbf{x}} = \mathbf{U}^T \mathbf{x} = \left[\sum_{j=1}^N u_{1j} x_j, \dots, \sum_{j=1}^N u_{Nj} x_j \right]^T \in \mathbb{R}^N, \quad (5)$$

where the i -th element $\widehat{x}_i = \sum_{j=1}^N u_{ij} x_j = \langle \mathbf{u}_i, \mathbf{x} \rangle$ denotes the signal strength of the spectral signal corresponding to the eigenvalue λ_i in the spectral domain. Then, based upon them, the spectral graph convolution is defined as:

$$\mathbf{g}_\theta \mathbf{U}^T \mathbf{x} = [g_\theta(\lambda_1) \widehat{x}_1, \dots, g_\theta(\lambda_N) \widehat{x}_N]^T \in \mathbb{R}^N. \quad (6)$$

Finally, the inverse Fourier transform is used to map the spectral signal back to the spatial domain:

$$\begin{aligned} \mathbf{L}_{sym} \mathbf{x} &= \mathbf{U} \mathbf{g}_\theta \mathbf{U}^\top \mathbf{x} = [\mathbf{u}_1, \dots, \mathbf{u}_N] [g_\theta(\lambda_1) \widehat{\mathbf{x}}_1, \dots, g_\theta(\lambda_N) \widehat{\mathbf{x}}_N]^\top \\ &= \sum_{i=1}^N g_\theta(\lambda_i) \widehat{\mathbf{x}}_i \mathbf{u}_i \in \mathbb{R}^N. \end{aligned} \quad (7)$$

Remark 1. *The connection between graph and wave.* From Eq. (7), we can observe that the graph signal in *spatial* domain can be treated as a linear combination of N different eigenvalues in *spectral* domain, vividly depicted in Figure 1 (Top). Intuitively, we can interpret the eigenvalue λ_i as the frequency, its corresponding eigenvector \mathbf{u}_i as a particular type of wave, and $g_\theta(\lambda_i) \widehat{\mathbf{x}}_i$ denotes the amplitude of the wave. This reflects the wave nature of the spectral graph convolution on any given graphs.

3.2 Graph Wave Equation

We are going to extend the wave equation on the graph. Given the graph signal $\mathbf{X} \in \mathbb{R}^{N \times d}$ (i.e., node features), for any node v_i , its node representation acquires messages from its neighbors $v_j \in \mathcal{N}(v_i)$ in GNNs. Then, we can derive the gradient of v_i in MP on its graph G by vector subtraction between v_i and its neighbors, which actually captures their signal differences [6]:

$$\nabla_G \mathbf{x}_i := [\dots, \mathbf{x}_i - \mathbf{x}_j, \dots]^\top \in \mathbb{R}^{|\mathcal{N}(v_i)| \times d}, \quad (8)$$

where the gradient direction reflects the direction from v_j to v_i in MP, and the gradient magnitude measures the feature difference amount between v_i and v_j . Subsequently, we can derive the divergence of v_i on G by the sum of feature differences between the node v_i and all its neighbor $v_j \in \mathcal{N}(v_i)$:

$$\text{div}_G(\nabla_G \mathbf{x}_i) := \sum_{v_j \in \mathcal{N}(v_i)} (\mathbf{x}_i - \mathbf{x}_j) \in \mathbb{R}^d, \quad (9)$$

where the divergence actually measures the total difference between a node and its neighborhood. Finally, by substituting Eq. (9) into (4), we propose **Graph Wave Equation** on the graph:

$$\frac{\partial^2 \mathbf{X}}{\partial t^2} = a^2 [\dots, \text{div}_G(\nabla_G \mathbf{x}_i), \dots]^\top \in \mathbb{R}^{N \times d}. \quad (10)$$

where \mathbf{X} is the signal intensity (of all nodes) in the entire graph G , and can be regarded as the node representations. Each row of \mathbf{X} involves a wave equation at a specific node. By introducing the form of Laplacian, we can rewrite Eq. (10) as follows (see Appendix A.1 for mathematical proof):

Proposition 1. Let $\mathbf{L} = \mathbf{D} - \mathbf{A}$ denote the discrete form of the Laplacian operator Δ . The *graph wave equation* can be rewritten as:

$$\frac{\partial^2 \mathbf{X}}{\partial t^2} = a^2 \mathbf{L} \mathbf{X} := \mathbf{L}_a \mathbf{X}. \quad (11)$$

where we incorporate a into \mathbf{L} for a simple form, i.e., $\mathbf{L}_a := a^2 \mathbf{L}$. Here, the propagation velocity a controls the speed of wave propagation between nodes on the graph. Note that the propagation velocity a can alternatively be constant or learnable parameters in practice, leading to different forms of Laplacian (detailed in Eq. (15) and (17) later). Benefit by treating a as learnable parameters, we can redefine Laplacian with flexibility and establish a connection between wave equation and Laplacian-based spectral GNNs.

Remark 2. *The connection between graph wave equation and spectral GNNs.* With Eq. (11), we can easily combine the wave equation with spectral GNNs into graph wave equations. Thereby, the graph wave equation can be flexibly extended and achieved by specific designed Laplacians of existing spectral GNNs.

3.3 Solution of Graph Wave Equation

In general, it is often intractable to obtain an analytical solution for a PDE. Fortunately, there are numerical methods that can approximate PDE solutions. First, the continuous PDE can be discretized into a finite form of a linear algebraic system using the finite difference method. Then, an iteration process with initial values can be employed to solve this linear algebraic system. In the context of graphs, only the time dimension needs to be further discretized on each node. To this end, we employ a commonly-used discretization method in mathematics, namely *forward Euler method*, to solve the graph wave equation for node representations (i.e., \mathbf{X}) [6].

Formally, the forward Euler method discretizes the graph wave equation by performing forward difference in the time dimension, and then derives the **explicit scheme**:

$$\frac{\mathbf{X}^{(n+1)} - 2\mathbf{X}^{(n)} + \mathbf{X}^{(n-1)}}{\tau^2} = \mathbf{L}_a^{(n)} \mathbf{X}^{(n)}, \quad (12)$$

where τ is the time step length. The initial values of $\mathbf{X}^{(0)}$ and $\mathbf{X}^{(1)}$ in the PDE can be obtained using the second-order central quotient:

$$\mathbf{X}^{(0)} = \varphi_0(\mathbf{X}), \quad \mathbf{X}^{(1)} = \tau \varphi_1(\mathbf{X}) + \left(\mathbf{I} + \frac{\tau^2}{2} \mathbf{L}_a^{(0)} \right) \varphi_0(\mathbf{X}), \quad (13)$$

where $\varphi_0(\mathbf{X})$ and $\varphi_1(\mathbf{X})$ can be practically achieved by neural networks, such as feedforward networks. Finally, the explicit scheme of the graph wave equation is given by:

$$\mathbf{X}^{(n+1)} = \left(2\mathbf{I} + \tau^2 \mathbf{L}_a^{(n)} \right) \mathbf{X}^{(n)} - \mathbf{X}^{(n-1)}. \quad (14)$$

Please see Appendix A.2 for the detailed derivation of the forward Euler method. In particular, we can interpret the above equation from the perspective of message passing:

Remark 3. *The perspective of message passing.* By decomposing $\mathbf{X}^{(n+1)}$ into $\mathbf{X}^{(n+1)} = \left(\mathbf{I} + \tau^2 \mathbf{L}_a^{(n)} \right) \mathbf{X}^{(n)} + \left(\mathbf{X}^{(n)} - \mathbf{X}^{(n-1)} \right)$, the graph signal at time t_{n+1} consists of two components: 1) the aggregation of neighbor information at time t_n , and 2) the difference between the graph signal at times t_n and t_{n-1} .

3.4 Graph Wave Networks

In this section, we propose two specifications of GWNs with time-independent and time-dependent Laplacian, respectively.

Symmetric Normalized Laplacian. We consider time-independent Laplacian, where we let the velocity be a constant. Typically, we adopt GCN [20] as the base model and design a symmetric normalized Laplacian without self-loops, which behaves as a low-pass filter in the spectral domain:

$$\mathbf{L}_a = \mathbf{D}^{-\frac{1}{2}} \mathbf{A} \mathbf{D}^{-\frac{1}{2}}. \quad (15)$$

GWN-sym. We propose the Graph Wave Network based on the symmetric normalized Laplacian. With the initial values given by

Eq. (13), the feature matrix at time t_{n+1} can be determined as:

$$\mathbf{X}^{(n+1)} = \left(2\mathbf{I} + \tau^2 \mathbf{D}^{-\frac{1}{2}} \mathbf{A} \mathbf{D}^{-\frac{1}{2}}\right) \mathbf{X}^{(n)} - \mathbf{X}^{(n-1)}. \quad (16)$$

The final feature matrix at the terminal time T is transformed into a prediction matrix by an MLP as $\mathbf{Y} = \text{MLP}(\mathbf{X}^{(T)})$.

Frequency Adaptive Laplacian. Next, we consider time-dependent Laplacian, where the velocity is non-constant learnable parameters. Typically, we adopt FAGCN [3] as the base model and propose a frequency adaptive Laplacian with a time-dependent learnable parameter $\varepsilon^{(n)} \in (0, 1)$, which designs both a low-pass filter and a high-pass filter in the spectral domain:

$$\mathbf{L}_{a,l}^{(n)} = \varepsilon^{(n)} \mathbf{I} + \mathbf{D}^{-\frac{1}{2}} \mathbf{A} \mathbf{D}^{-\frac{1}{2}}, \quad \mathbf{L}_{a,h}^{(n)} = \varepsilon^{(n)} \mathbf{I} - \mathbf{D}^{-\frac{1}{2}} \mathbf{A} \mathbf{D}^{-\frac{1}{2}}. \quad (17)$$

GWN-fa. We propose the Graph Wave Network based on the frequency adaptive Laplacian. The initial values are also given by Eq. (13), and the feature matrix at time t_{n+1} can be determined as (see Appendix A.4 for detailed derivation):

$$\mathbf{X}^{(n+1)} = \varepsilon^{(n)} \mathbf{X}^{(0)} + \left(2\mathbf{I} + \tau^2 \boldsymbol{\alpha}^{(n)} \odot \mathbf{D}^{-\frac{1}{2}} \mathbf{A} \mathbf{D}^{-\frac{1}{2}}\right) \mathbf{X}^{(n)} - \mathbf{X}^{(n-1)}. \quad (18)$$

where the element $\alpha_{ij}^{(n)} = \tanh(\mathbf{g}^{(n)\top} [\mathbf{x}_i^{(n)} \parallel \mathbf{x}_j^{(n)}])$ of $\boldsymbol{\alpha}^{(n)}$ is the attention weight between nodes v_i and v_j at time t_n , and $\mathbf{g}^{(n)} \in \mathbb{R}^{2d}$ is a learnable parameter vector. Notably, when $\alpha_{ij}^{(n)} > 0$, the two nodes are more similar and GWN-fa behaves a low-pass filter; and when $\alpha_{ij}^{(n)} < 0$, two nodes are more dissimilar and GWN-fa behaves a high-pass filter. The final feature matrix at terminal time T is also transformed into a prediction matrix by an MLP.

3.5 Stability

Stability is an important property of differential equations, which is closely related to the robustness in machine learning [6], and refers to the property that small perturbations in initial values would not result in a significant change in solutions. We discuss the initial value stability of the explicit scheme $\mathbf{U}^{(k+1)} = \mathbf{C}\mathbf{U}^{(k)}$. Formally, if there exists $\tau_0 > 0$ and a constant $K > 0$ such that the inequality $\|\mathbf{U}^{(k+1)}\| = \|\mathbf{C}^{k+1}\mathbf{U}^{(0)}\| \leq K\|\mathbf{U}^{(0)}\|$ holds for all $0 < \tau \leq \tau_0$ and $0 < k\tau \leq T$, then the explicit scheme is said to be initial value stable. It is crucial to prove the stability of explicit schemes to ensure that the resulting GNNs is reliable and feasible. A commonly used method for proving stability is the matrix method:

Theorem 1. Let $\rho(\mathbf{C}) = |\lambda|_{\max}$ denote the spectral radius of matrix \mathbf{C} , if $\rho(\mathbf{C}) \leq 1$, the numerical scheme is stable.

Based on Theorem 1, we prove that both the explicit schemes based on the symmetric normalized Laplacian (see Appendix A.3 for proof) and the frequency adaptive Laplacian (see Appendix A.5 for proof) are **constantly stable**.

Theorem 2. Given $\mathbf{L}_a = \mathbf{D}^{-1/2} \mathbf{A} \mathbf{D}^{-1/2}$ with $\lambda \in [-1, 1]$, the explicit scheme is constantly stable for any $\tau \in \mathbb{R}^+$.

Theorem 3. Given $\mathbf{L}_{a,\cdot} = \varepsilon \mathbf{I} \pm \mathbf{D}^{-\frac{1}{2}} \mathbf{A} \mathbf{D}^{-\frac{1}{2}}$ with $\lambda \in [\varepsilon - 1, \varepsilon + 1]$, the explicit scheme is constantly stable for any $\tau \in \mathbb{R}^+$.

Remark 4. *The impact of constantly stability for models.* Theoretically, we prove that the explicit scheme of the graph wave equation is constantly stable, guaranteeing the model performance would not be affected by the time step length, thus allowing to improve the efficiency by choosing a relatively larger τ .

Comparison with heat equation based GRAND. The explicit scheme of GRAND is $\mathbf{X}^{(n+1)} = \left(\mathbf{I} + \tau \bar{\mathbf{A}}(\mathbf{X}^{(n)})\right) \mathbf{X}^{(n)}$, where $\bar{\mathbf{A}}(\mathbf{X}^{(n)})$ is an attention matrix constrained to be a right stochastic matrix satisfying $\sum_{j=1}^N \alpha_{ij} = 1$ and $\alpha_{ij} > 0$. Benefiting from being a right stochastic matrix, the explicit scheme is stable and can be directly proven. However, it has the two deficiencies: First, the stability of explicit schemes is conditional (*i.e.*, $0 < \tau < 1$), striking a balance between performance and efficiency. Detailed comparisons and validations can be found in Sec. 4.4. Second, the attention scores are constrained to $\alpha_{ij} > 0$, which performs poorly in distinguishing inter-class nodes. In contrast, our GWN-fa acts as low-pass and high-pass filters when $\alpha_{ij} > 0$ and $\alpha_{ij} < 0$ respectively, enabling better handling of various types of graph.

3.6 Complexity Analysis

The number of learnable parameters of GWN-sym and GWN-fa are $2fd + dc$ and $2fd + (2d + 1)T/\tau + dc$, compared to $fd + 2d^2 + dc$ in GRAND [6]. Here, f , d and c denote the input dimension, the hidden layer dimension, and the number of classes, respectively. In general, $T/\tau < d$. The computational complexity of each layer of GWN-sym and GWN-fa are $\mathcal{O}(Md)$ and $\mathcal{O}((N + M)d)$, compared to $\mathcal{O}(M'd)$ in GRAND. Here, N , M and M' are the number of nodes, edges and rewritten edges.

4 Experiments

4.1 Experimental Setup

Datasets. Following the practices [6, 36], we conduct node classification [37] on the following real-world datasets (see Appendix B.1 for statistics): (1) *homophilic datasets* [37, 52]: citation networks Cora, CiteSeer and PubMed, Amazon co-purchase networks Computers and Photo, and co-author networks CS; (2) *heterophilic datasets* [31, 33–35]: co-occurrence graph Actor, WebKB datasets Texas, Cornell and Wisconsin, and social network DeezerEurope; (3) *large-scale dataset* [18]: citation network ogbn-arxiv.

Baselines. We categorize all baselines into the following two classes: (1) *mainstream GNNs*: GCN [20], GAT [43], GraphSAGE [15], SGC [46], JK-Net [50], ResGCN [22], GCNII [7], FAGCN [3], GPR-GNN [9], AIR [53], MixHop [1], Geom-GCN [31], H₂GCN [56], LINKX [26], WRGAT [41], GGCN [51], NLMLP [28], GloGNN [23], NSD [4], ACM-GCN [29], Ordered GNN [40]; (2) *GNNs based on differential equation*: GDC [21], CGNN [49], ADC [54], GADC [54], GRAND [6], GraphCON [36]. Unless specifically state that the results are from original papers, baselines are reproduced using their open-source code with fair settings.

Setup. We split the datasets into training/validation/test sets using two schemes: 60%/20%/20% [3, 9] and 48%/32%/20% [4, 31, 51, 56]. During the training phase, our method utilizes the cross-entropy loss function, Adam optimizer [19], and early stopping strategy. The code is implemented using the PyTorch Geometric library [12] and parameter search is performed using wandb library. Finally, we report the mean accuracy and standard deviation of 10 runs.

4.2 Performance

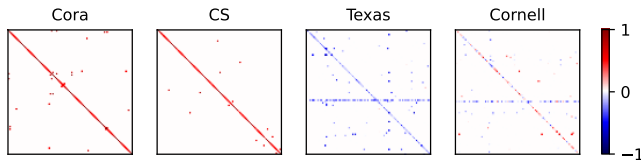
To validate the feasibility of GWN, we first compare it with GNNs based on differential equations on 6 homophilic graphs. Table 2

Table 2: The results of homophilic datasets and large-scale dataset: mean accuracy \pm standard deviation on 60%/20%/20% random splits of data and 10 runs. * models use the best variants, – indicate the paper did not report this result, † using 1.5M parameters.

Datasets	Cora	CiteSeer	PubMed	Computers	Photo	CS	obgn-arxiv
GCN	87.51 \pm 1.38	80.59 \pm 1.12	87.95 \pm 0.83	86.09 \pm 0.61	93.04 \pm 0.53	95.14 \pm 0.25	72.17 \pm 0.33
GAT	87.42 \pm 1.46	80.16 \pm 1.63	85.91 \pm 1.26	87.89 \pm 0.82	93.53 \pm 0.58	94.37 \pm 0.28	73.65 \pm 0.11 †
GraphSAGE	87.50 \pm 1.45	79.39 \pm 1.38	89.64 \pm 0.73	88.53 \pm 0.70	94.49 \pm 0.55	95.93 \pm 0.25	71.39 \pm 0.16
GDC	86.89 \pm 1.28	80.05 \pm 0.60	86.18 \pm 0.42	88.56 \pm 0.38	93.56 \pm 0.33	94.82 \pm 0.22	–
CGNN	88.29 \pm 1.11	79.93 \pm 1.04	89.46 \pm 0.52	88.31 \pm 0.65	94.35 \pm 0.56	96.21 \pm 0.32	58.70 \pm 2.50
ADC*	87.45 \pm 0.89	79.43 \pm 0.96	90.23 \pm 0.39	88.62 \pm 0.56	95.33 \pm 0.27	95.82 \pm 0.15	–
GADC	87.64 \pm 0.64	78.62 \pm 0.57	88.58 \pm 0.48	87.78 \pm 0.54	94.70 \pm 0.35	96.16 \pm 0.29	–
GRAND*	88.70 \pm 0.99	<u>81.56 \pm 1.28</u>	88.39 \pm 0.32	89.37 \pm 0.41	95.79 \pm 0.59	95.77 \pm 0.28	72.23 \pm 0.20
GraphCON*	87.81 \pm 0.92	79.68 \pm 1.23	88.54 \pm 1.32	–	–	–	–
GWN-sym	<u>89.61 \pm 0.87</u>	81.81 \pm 1.70	<u>90.56 \pm 0.54</u>	<u>90.10 \pm 0.87</u>	95.31 \pm 0.65	<u>96.66 \pm 0.26</u>	72.19 \pm 0.20
GWN-fa	89.66 \pm 1.29	80.89 \pm 1.51	90.64 \pm 0.73	90.62 \pm 0.61	<u>95.61 \pm 0.53</u>	96.67 \pm 0.26	<u>72.40 \pm 0.10</u>

Table 3: The results of heterophilic datasets: mean accuracy \pm standard deviation on 10 runs. * models use the best variants, † results of baselines from papers, ‡ results of baselines are reproduced, – indicate the original paper did not report this result.

Datasets Splits	Actor	Texas		Cornell		Wisconsin		DeezerEurope
	60/20/20(%)†	48/32/20(%)†	60/20/20(%)‡	48/32/20(%)†	60/20/20(%)‡	48/32/20(%)†	60/20/20(%)‡	60/20/20(%)†
GCN	27.32 \pm 1.10	55.14 \pm 5.16	79.33 \pm 4.47	60.54 \pm 5.30	69.53 \pm 11.79	51.76 \pm 3.06	63.94 \pm 4.93	62.23 \pm 0.53
GAT	27.44 \pm 0.89	52.16 \pm 6.63	79.59 \pm 9.21	61.89 \pm 5.05	66.91 \pm 15.99	49.41 \pm 4.09	63.45 \pm 11.65	61.09 \pm 0.77
GraphSAGE	34.23 \pm 0.99	82.43 \pm 6.14	86.02 \pm 4.78	75.95 \pm 5.01	85.06 \pm 5.12	81.18 \pm 5.56	89.56 \pm 3.99	–
MixHop	32.22 \pm 2.34	77.84 \pm 7.73	–	73.51 \pm 6.34	–	75.88 \pm 4.90	–	66.80 \pm 0.58
Geom-GCN	31.59 \pm 1.15	66.76 \pm 2.72	–	60.54 \pm 3.67	–	64.51 \pm 3.66	–	–
H ₂ GCN	35.70 \pm 1.00	84.86 \pm 7.23	85.90 \pm 3.53	82.70 \pm 5.28	86.23 \pm 4.71	87.65 \pm 4.98	87.50 \pm 1.77	67.22 \pm 0.90
LINKX	36.10 \pm 1.55	74.60 \pm 8.37	–	77.84 \pm 5.81	–	75.49 \pm 5.72	–	–
WRGAT	36.53 \pm 0.77	83.62 \pm 5.50	–	81.62 \pm 3.90	–	86.98 \pm 3.78	–	–
FACGN	34.82 \pm 1.35	82.43 \pm 6.89	85.57 \pm 4.75	79.19 \pm 9.79	86.38 \pm 5.33	82.94 \pm 7.95	84.88 \pm 9.19	66.86 \pm 0.53
GPR-GNN	35.16 \pm 0.90	78.38 \pm 4.36	91.89 \pm 4.08	80.27 \pm 8.11	85.91 \pm 4.60	82.94 \pm 4.21	93.84 \pm 3.16	66.90 \pm 0.50
GGCN	37.54 \pm 1.56	84.86 \pm 4.55	<u>92.13 \pm 3.05</u>	85.68 \pm 6.63	88.70 \pm 4.97	86.86 \pm 3.29	<u>94.56 \pm 3.26</u>	–
NLMLP	–	85.40 \pm 3.80	–	84.90 \pm 5.70	–	87.30 \pm 4.30	–	–
GloGNN*	37.70 \pm 1.40	84.05 \pm 4.90	–	85.95 \pm 5.10	–	88.04 \pm 3.22	–	–
NSD*	37.81 \pm 1.15	85.95 \pm 5.51	–	84.86 \pm 4.71	–	89.41 \pm 4.74	–	–
ACM-GCN*	37.31 \pm 1.09	88.38 \pm 3.43	–	86.49 \pm 6.73	–	88.43 \pm 3.66	–	67.50 \pm 0.53
Ordered GNN	37.99 \pm 1.70	86.22 \pm 4.12	90.82 \pm 4.18	87.03 \pm 4.73	88.09 \pm 3.36	88.04 \pm 3.63	93.62 \pm 2.91	–
GWN-sym	<u>39.97 \pm 1.72</u>	<u>89.85 \pm 5.05</u>	91.64 \pm 3.74	<u>88.11 \pm 3.17</u>	<u>89.57 \pm 3.54</u>	<u>90.88 \pm 4.43</u>	93.38 \pm 3.18	<u>68.15 \pm 0.77</u>
GWN-fa	42.03 \pm 1.59	92.94 \pm 4.45	93.28 \pm 3.14	90.81 \pm 4.63	92.13 \pm 3.76	94.26 \pm 1.76	95.63 \pm 1.59	68.63 \pm 0.29

**Figure 2: Visualization of the attention matrix α of GWN-fa.**

indicates that GWN outperforms heat equation based methods such as GRAND on 5 datasets and achieves suboptimal performance on Photo. Since both GWN-sym and GWN-fa can be treated as low-pass filters, their performances are closely comparable. Then, we examine the generality of GWN on heterophilic graphs. Table 3 demonstrates

that GWN outperforms state-of-the-art methods under two commonly used data splits. GWN-sym and GWN-fa show a significant difference on heterophilic graphs, which can be attributed to the high-pass filter of GWN-fa. *It reflects remarkable performance in modelling heterophily in graphs.* Next, we further probe whether the low-pass and high-pass filters in GWN-fa perform as expected. As shown in Figure 2, we visualize the attention matrix α in Eq. (18). As stated in Sec. 3.4, GWN behaves as a low-pass filter when $\alpha_{ij} > 0$ and behaves as a high-pass filter when $\alpha_{ij} < 0$. This is consistent with the visualized results. Additionally, it is worth noting that under the 48%/32%/20% split, GWN-fa even outperforms most state-of-the-art methods under the 60%/20%/20% split, highlighting its superiority in scenarios with low label rates. Furthermore, GWNs also achieve competitive performance on obgn-arxiv, demonstrating its scalability on large-scale graphs.

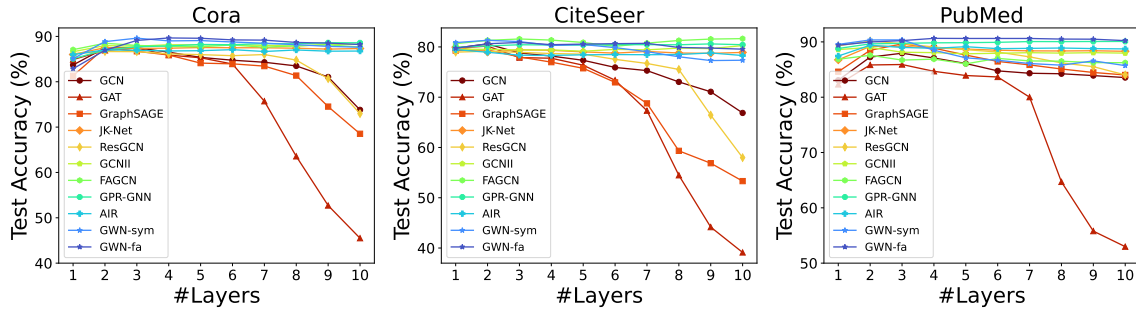


Figure 3: Performances of methods of each layer on citation networks.

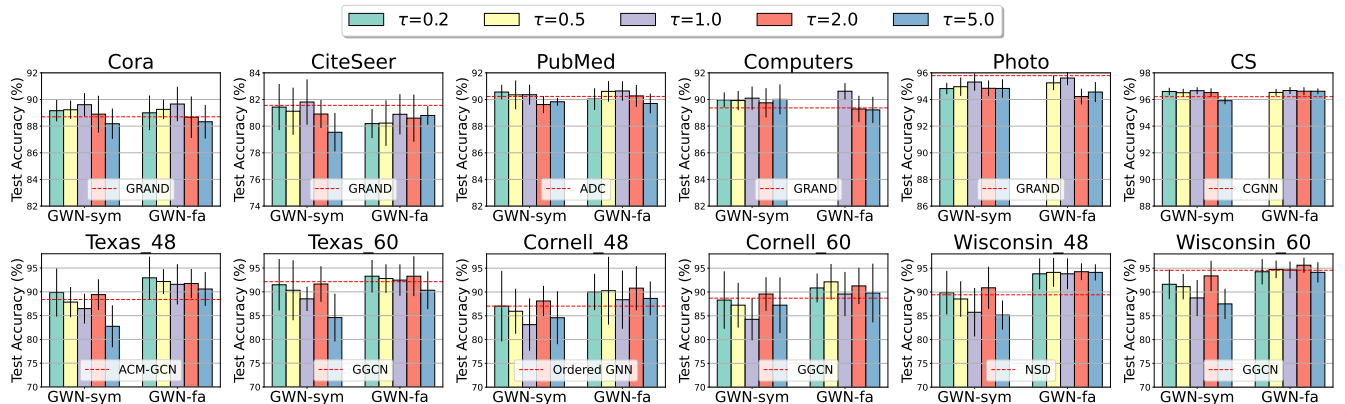


Figure 4: Stability analysis of GWN. Red dashed line indicates the SOTA models.

Table 4: Comparison with base models using best parameters.

	Cora	CiteSeer	PubMed	Computers	Photo	CS	Texas	Cornell	Wisconsin
GCN	87.51	80.59	87.95	86.09	93.04	95.14	79.33	69.53	63.94
GWN-sym	89.61 (\uparrow 2.10)	81.81 (\uparrow 1.22)	90.56 (\uparrow 2.61)	90.10 (\uparrow 4.01)	95.31 (\uparrow 2.27)	96.66 (\uparrow 1.52)	91.64 (\uparrow 12.31)	89.57 (\uparrow 20.04)	93.38 (\uparrow 29.44)
FAGCN	88.49	81.65	87.58	87.32	93.41	95.79	85.57	86.38	84.88
GWN-fa	89.66 (\uparrow 1.17)	80.89 (\downarrow 0.76)	90.64 (\uparrow 3.06)	90.62 (\uparrow 3.30)	95.61 (\uparrow 2.20)	96.67 (\uparrow 0.88)	93.28 (\uparrow 7.71)	92.13 (\uparrow 5.75)	95.63 (\uparrow 10.75)

4.3 Over-smoothing Analysis

We investigate the ability of GWN to mitigate over-smoothing on three citation networks: Cora, CiteSeer, and PubMed. Following the practice of Chamberlain et al. [6] and Rusch et al. [36], we set $\tau = 1$, then the terminal time T denotes the number of layers. Figure 3 demonstrates that compared to GNNs specifically designed for over-smoothing, GWN not only outperforms all baselines in terms of performance but also maintains its performance as the number of layers increases. It demonstrates that *our models have better performance in mitigating the over-smoothing issue.*

4.4 Stability Analysis

We analyze the stability of the explicit scheme in experiments. We run GWN on all datasets and report the accuracy for different τ . As depicted in Figure 4, on larger-scale datasets such as CS, GWN exhibits minimal performance differences when τ is varied. On

smaller-scale datasets like Texas, due to the high-pass filters, GWN-fa demonstrates better stability compared to GWN-sym. Compared to GRAND, which only guarantees stability of the explicit scheme for $\tau = 0.005$ [6], *GWN can maintain stability at larger τ while achieving higher computational efficiency and performance.*

4.5 Analysis of base models

We explore the impact of base models in Table 4, where both GCN and FAGCN increase their performances in the form of the graph wave equation. Besides, we also show the visualization of wave propagation of GWN-sym and GWN-fa on Cora. From Figure 5, the waveform of GWN-sym are not prominent at early iterations, while the waveform of GWN-fa demonstrate more frequent information interactions at any time. Figure 6(a) depicts wave signals at a specific time, where the waveform of GWN-sym appears chaotic, whereas the waveform of GWN-fa is relatively clear. From Figure 6(b), compared to the waveform of GWN-sym, the waveform of GWN-fa exhibits periodic variations of peaks and troughs. We

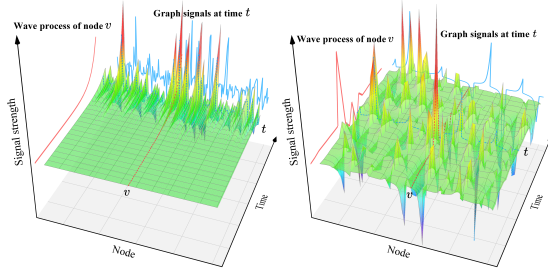


Figure 5: Visualization of waveform in wave propagation of GWN-sym (Left) and GWN-fa (Right) on Cora.

believe that these phenomena can be attributed to the ability of capturing both the low- and high-frequency signals in GWN-fa.

5 Related Work

Spectral GNNs. Spectral GNNs [5] based on Laplacian to design various filter functions in the spectral domain. One category of spectral GNNs directly modify the Laplacian. GCN [20] incorporates self-loops in the normalized Laplacian, which manifests as a low-pass filter. Some methods [3, 14, 29, 55] introduce additional high-pass filters to learn difference between nodes. Bianchi et al. [2] propose an auto-regressive moving average filter to capture the global graph structure. Defferrard et al. [10] and He et al. [17] approximate the spectral graph convolution using Chebyshev polynomial. He et al. [16] approximate arbitrary filters using Bernstein polynomials. Wang and Zhang [44] utilize Jacobi polynomials to adapt a wider range of weight functions. Chien et al. [9] employ learnable parameters to approximate the polynomial coefficients. *These methods are all built upon the traditional graph signal processing methods, but few of them fully explore the nature of wave propagation in the MP process.*

Differential Equations on Graphs. Neural ODE [8] models the embedding representation as a continuous dynamic with respect to neural network parameters. Poli et al. [32] propose a continuous-depth GNN framework and solves the forward process using numerical methods. Khonneux et al. [49] establish the relationship between the derivative of node embeddings and the initial and neighboring embeddings of nodes. Rusch et al. [36] relate to traditional GNNs using second-order ODEs. Nguyen et al. [30] adapt well-known Kuramoto model to alleviate over-smoothing. Neural PDE [25] applies partial differential equations to graph-based problems. Eliasof et al. [11] utilizes non-linear diffusion and non-linear hyperbolic equations to model message passing. Wang et al. [45] decouple the terminal time and feature propagation steps from a continuous perspective. Klicpera et al. [21] define graph diffusion convolution to overcome the limitation of traditional GNNs in aggregating only direct neighbors. Zhao et al. [54] propose adaptive diffusion convolution to automatically learn the optimal neighborhood from the data. Recent works introduce the heat diffusion equation on graphs to simulate the temporal dynamics of node embeddings [6]. The explicit scheme stability derived from GRAND is conditional, ensuring model performance only when using smaller time steps, leading to inefficient model performance. Thorpe et al.

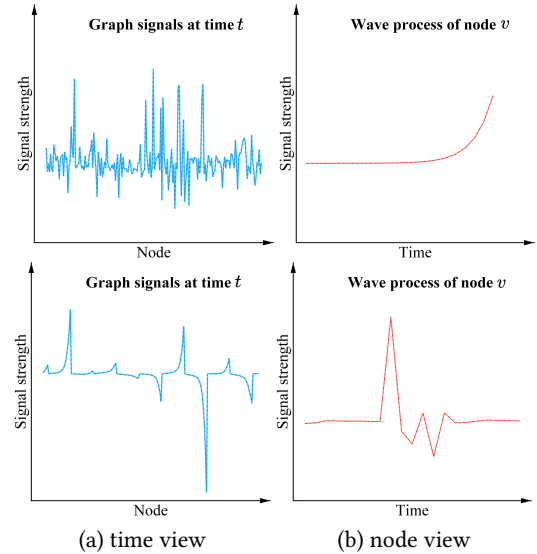


Figure 6: Visualization of time and node view in wave propagation of GWN-sym (Up) and GWN-fa (Down) on Cora.

[42] further utilize a heat diffusion equation with a source term to define graph convolution, which performs better in low-label-rate scenarios. Li et al. [24] introduce a general diffusion equation framework with a fidelity term and establishes the connection between the diffusion process and GNNs. Compared to considering message passing as a heat diffusion process between nodes, treating it as a wave propagation process better aligns with the process of inter-node information interaction described in graph signal processing. Moreover, note that there are several DE-based GNNs [11, 24, 42, 45, 49] lack stability proofs, which can hardly ensure the robustness of models, and weaker stability conditions make it challenging to balance model performance and efficiency. *In contrast, in this paper, the proposed graph wave networks can significantly enhance efficiency while ensuring model performance, due to its constantly stable properties.*

6 Conclusion

In this paper, we consider the message passing in GNNs as a wave propagation process, and further develop graph wave networks (GWNs) based on the proposed graph wave equation with spectral GNNs. We demonstrate that compared to the heat equation, the graph wave equation exhibits superior performance and stability. Extensive experiments demonstrate that our GWNs obtain accurate and efficient performance, and show effectiveness in addressing challenging graph problems such as over-smoothing and heterophily modelling. Our future work would explore more complex and general Laplacian polynomials to advance GNNs.

Acknowledgments

This work is supported by the National Natural Science Foundation of China (No.62406319 and No.62472416), the Youth Innovation Promotion Association of CAS (Grant No. 2021153), and the Post-doctoral Fellowship Program of CPSF (No.GZC20232968).

References

- [1] Sami Abu-El-Hajja, Bryan Perozzi, Amol Kapoor, Nazanin Alipourfard, Kristina Lerman, Hrayr Harutyunyan, Greg Ver Steeg, and Aram Galstyan. 2019. MixHop: Higher-Order Graph Convolutional Architectures via Sparsified Neighborhood Mixing. In *Proceedings of the 36th International Conference on Machine Learning, ICML 2019, 9–15 June 2019, Long Beach, California, USA*. PMLR.
- [2] Filippo Maria Bianchi, Daniele Grattarola, Lorenzo Livi, and Cesare Alippi. 2022. Graph Neural Networks With Convolutional ARMA Filters. *IEEE Trans. Pattern Anal. Mach. Intell.* 44, 7 (2022), 3496–3507. doi:10.1109/TPAMI.2021.3054830
- [3] Deyu Bo, Xiao Wang, Chuan Shi, and Huawei Shen. 2021. Beyond Low-frequency Information in Graph Convolutional Networks. In *Thirty-Fifth AAAI Conference on Artificial Intelligence, AAAI 2021, Thirty-Third Conference on Innovative Applications of Artificial Intelligence, IAAI 2021, The Eleventh Symposium on Educational Advances in Artificial Intelligence, EAAI 2021, Virtual Event, February 2–9, 2021*. AAAI Press.
- [4] Cristian Bodnar, Francesco Di Giovanni, Benjamin Paul Chamberlain, Pietro Lió, and Michael M. Bronstein. 2022. Neural Sheaf Diffusion: A Topological Perspective on Heterophily and Oversmoothing in GNNs. In *NeurIPS*.
- [5] Joan Bruna, Wojciech Zaremba, Arthur Szlam, and Yann LeCun. 2014. Spectral Networks and Locally Connected Networks on Graphs. In *2nd International Conference on Learning Representations, ICLR 2014, Banff, AB, Canada, April 14–16, 2014, Conference Track Proceedings*, Yoshua Bengio and Yann LeCun (Eds.). <http://arxiv.org/abs/1312.6203>
- [6] Ben Chamberlain, James Rowbottom, Maria I. Gorinova, Michael M. Bronstein, Stefan Webb, and Emanuele Rossi. 2021. GRAND: Graph Neural Diffusion. In *Proceedings of the 38th International Conference on Machine Learning, ICML 2021, 18–24 July 2021, Virtual Event (Proceedings of Machine Learning Research, Vol. 139)*, Marina Meila and Tong Zhang (Eds.). PMLR, 1407–1418. <http://proceedings.mlr.press/v139/chamberlain21a.html>
- [7] Ming Chen, Zhewei Wei, Zengfeng Huang, Bolin Ding, and Yaliang Li. 2020. Simple and Deep Graph Convolutional Networks. In *Proceedings of the 37th International Conference on Machine Learning, ICML 2020, 13–18 July 2020, Virtual Event*. PMLR.
- [8] Tian Qi Chen, Yulia Rubanova, Jesse Bettencourt, and David Duvenaud. 2018. Neural Ordinary Differential Equations. In *Advances in Neural Information Processing Systems 31: Annual Conference on Neural Information Processing Systems 2018, NeurIPS 2018, December 3–8, 2018, Montréal, Canada*, Samy Bengio, Hanna M. Wallach, Hugo Larochelle, Kristen Grauman, Nicolò Cesa-Bianchi, and Roman Garnett (Eds.). 6572–6583. <https://proceedings.neurips.cc/paper/2018/hash/69386f6bb1dfed6892a24c8686939b9-Abstract.html>
- [9] Eli Chien, Jianhao Peng, Pan Li, and Olgica Milenkovic. 2021. Adaptive Universal Generalized PageRank Graph Neural Network. In *9th International Conference on Learning Representations, ICLR 2021, Virtual Event, Austria, May 3–7, 2021*. OpenReview.net.
- [10] Michaël Defferrard, Xavier Bresson, and Pierre Vandergheynst. 2016. Convolutional Neural Networks on Graphs with Fast Localized Spectral Filtering. In *Advances in Neural Information Processing Systems 29: Annual Conference on Neural Information Processing Systems 2016, December 5–10, 2016, Barcelona, Spain*.
- [11] Moshe Eliasof, Eldad Haber, and Eran Treister. 2021. PDE-GCN: Novel Architectures for Graph Neural Networks Motivated by Partial Differential Equations. In *Advances in Neural Information Processing Systems 34: Annual Conference on Neural Information Processing Systems 2021, NeurIPS 2021, December 6–14, 2021, virtual*, Marc'Aurelio Ranzato, Alina Beygelzimer, Yann N. Dauphin, Percy Liang, and Jennifer Wortman Vaughan (Eds.). 3836–3849. <https://proceedings.neurips.cc/paper/2021/hash/1f9f9d8ff75205aa73ec83e543d8b571-Abstract.html>
- [12] Matthias Fey and Jan Eric Lenssen. 2019. Fast Graph Representation Learning with PyTorch Geometric. In *ICLR Workshop on Representation Learning on Graphs and Manifolds*.
- [13] Thomas Gaudelot, Ben Day, Arian R. Jamasb, Jyothish Soman, Cristian Regep, Gertrude Liu, Jeremy B. R. Hayter, Richard Vickers, Charles Roberts, Jian Tang, David Roblin, Tom L. Blundell, Michael M. Bronstein, and Jake P. Taylor-King. 2021. Utilizing graph machine learning within drug discovery and development. *Briefings Bioinform.* 22, 6 (2021). doi:10.1093/BIB/BBAB159
- [14] Haoyu Geng, Chao Chen, Yixuan He, Gang Zeng, Zhaobing Han, Hua Chai, and Junchi Yan. 2023. Pyramid Graph Neural Network: A Graph Sampling and Filtering Approach for Multi-scale Disentangled Representations. In *Proceedings of the 29th ACM SIGKDD Conference on Knowledge Discovery and Data Mining, KDD 2023, Long Beach, CA, USA, August 6–10, 2023*, Ambuj K. Singh, Yizhou Sun, Leman Akoglu, Dimitrios Gunopulos, Xifeng Yan, Ravi Kumar, Fatma Ozcan, and Jieping Ye (Eds.). ACM, 518–530. doi:10.1145/3580305.3599478
- [15] William L. Hamilton, Zhitaoying, and Jure Leskovec. 2017. Inductive Representation Learning on Large Graphs. In *Advances in Neural Information Processing Systems 30: Annual Conference on Neural Information Processing Systems 2017, December 4–9, 2017, Long Beach, CA, USA*.
- [16] Mingguo He, Zhewei Wei, Zengfeng Huang, and Hongteng Xu. 2021. BernNet: Learning Arbitrary Graph Spectral Filters via Bernstein Approximation. In *Advances in Neural Information Processing Systems 34: Annual Conference on Neural Information Processing Systems 2021, NeurIPS 2021, December 6–14, 2021, virtual*, Marc'Aurelio Ranzato, Alina Beygelzimer, Yann N. Dauphin, Percy Liang, and Jennifer Wortman Vaughan (Eds.). 14239–14251. <https://proceedings.neurips.cc/paper/2021/hash/76f1cfd7754a6e4fc3281bccc3d0902-Abstract.html>
- [17] Mingguo He, Zhewei Wei, and Ji-Rong Wen. 2022. Convolutional Neural Networks on Graphs with Chebyshev Approximation, Revisited. In *Advances in Neural Information Processing Systems 35: Annual Conference on Neural Information Processing Systems 2022, NeurIPS 2022, New Orleans, LA, USA, November 28–December 9, 2022*, Sanmi Koyejo, S. Mohamed, A. Agarwal, Danielle Belgrave, K. Cho, and A. Oh (Eds.). http://papers.nips.cc/paper_files/paper/2022/hash/2f9b3ee2bcea04b327c09d7e3145bd1e-Abstract-Conference.html
- [18] Weihua Hu, Matthias Fey, Marinka Zitnik, Yuxiao Dong, Hongyu Ren, Bowen Liu, Michele Catasta, and Jure Leskovec. 2020. Open Graph Benchmark: Datasets for Machine Learning on Graphs. In *Advances in Neural Information Processing Systems 33: Annual Conference on Neural Information Processing Systems 2020, NeurIPS 2020, December 6–12, 2020, virtual*, Hugo Larochelle, Marc'Aurelio Ranzato, Raia Hadsell, Maria-Florina Balcan, and Hsuan-Tien Lin (Eds.). <https://proceedings.neurips.cc/paper/2020/hash/fb60d411a5c5b72b2e7d3527cfc84fd0-Abstract.html>
- [19] Diederik P. Kingma and Jimmy Ba. 2015. Adam: A Method for Stochastic Optimization. In *3rd International Conference on Learning Representations, ICLR 2015, San Diego, CA, USA, May 7–9, 2015, Conference Track Proceedings*.
- [20] Thomas N. Kipf and Max Welling. 2017. Semi-Supervised Classification with Graph Convolutional Networks. In *5th International Conference on Learning Representations, ICLR 2017, Toulon, France, April 24–26, 2017, Conference Track Proceedings*. OpenReview.net.
- [21] Johannes Klicpera, Stefan Weissenberger, and Stephan Günnemann. 2019. Diffusion Improves Graph Learning. In *Advances in Neural Information Processing Systems 32: Annual Conference on Neural Information Processing Systems 2019, NeurIPS 2019, December 8–14, 2019, Vancouver, BC, Canada*, Hanna M. Wallach, Hugo Larochelle, Alina Beygelzimer, Florence d'Alché-Buc, Emily B. Fox, and Roman Garnett (Eds.). 13333–13345. <https://proceedings.neurips.cc/paper/2019/hash/23c894276a2c5a16470e6a31f4618d73-Abstract.html>
- [22] Guohao Li, Matthias Müller, Ali K. Thabet, and Bernard Ghanem. 2019. DeepGCNs: Can GCNs Go As Deep As CNNs?. In *2019 IEEE/CVF International Conference on Computer Vision, ICCV 2019, Seoul, Korea (South), October 27–November 2, 2019*. IEEE, 9266–9275. doi:10.1109/ICCV.2019.00936
- [23] Xiang Li, Renyu Zhu, Yao Cheng, Caihua Shan, Siqiang Luo, Dongsheng Li, and Weining Qian. 2022. Finding Global Homophily in Graph Neural Networks When Meeting Heterophily. In *International Conference on Machine Learning, ICML 2022, 17–23 July 2022, Baltimore, Maryland, USA (Proceedings of Machine Learning Research, Vol. 162)*, Kamalika Chaudhuri, Stefanie Jegelka, Le Song, Csaba Szepesvári, Gang Niu, and Sivan Sabato (Eds.). PMLR, 13242–13256. <https://proceedings.mlr.press/v162/li22ad.html>
- [24] Yibo Li, Xiao Wang, Hongrui Liu, and Chuan Shi. 2024. A Generalized Neural Diffusion Framework on Graphs. In *Thirty-Eighth AAAI Conference on Artificial Intelligence, AAAI 2024, Thirty-Sixth Conference on Innovative Applications of Artificial Intelligence, IAAI 2024, Fourteenth Symposium on Educational Advances in Artificial Intelligence, EAAI 2024, February 20–27, 2024, Vancouver, Canada*, Michael J. Wooldridge, Jennifer G. Dy, and Sriraam Natarajan (Eds.). AAAI Press, 8707–8715. doi:10.1609/AAAI.V38I8.28716
- [25] Zongyi Li, Nikola B. Kovachki, Kamyar Aizzadenesheli, Burigede Liu, Andrew M. Stuart, Kaushik Bhattacharya, and Anima Anandkumar. 2020. Multiple Graph Neural Operator for Parametric Partial Differential Equations. In *Advances in Neural Information Processing Systems 33: Annual Conference on Neural Information Processing Systems 2020, NeurIPS 2020, December 6–12, 2020, virtual*, Hugo Larochelle, Marc'Aurelio Ranzato, Raia Hadsell, Maria-Florina Balcan, and Hsuan-Tien Lin (Eds.). <https://proceedings.neurips.cc/paper/2020/hash/4b21cf96d4cf612f239ac6322b10c8fe-Abstract.html>
- [26] Derek Lim, Felix Hohne, Xiuyu Li, Sijia Linda Huang, Vaishnavi Gupta, Omkar Bhalerao, and Ser-Nam Lim. 2021. Large Scale Learning on Non-Homophilous Graphs: New Benchmarks and Strong Simple Methods. In *Advances in Neural Information Processing Systems 34: Annual Conference on Neural Information Processing Systems 2021, NeurIPS 2021, December 6–14, 2021, virtual*, Marc'Aurelio Ranzato, Alina Beygelzimer, Yann N. Dauphin, Percy Liang, and Jennifer Wortman Vaughan (Eds.). 20887–20902. <https://proceedings.neurips.cc/paper/2021/hash/ae816a80e4c1c56caa2eb4e1819cbb2f-Abstract.html>
- [27] Jianghao Lin, Weiwen Liu, Xinyi Dai, Weinan Zhang, Shuai Li, Ruiming Tang, Xiuqiang He, Jianye Hao, and Yong Yu. 2021. A Graph-Enhanced Click Model for Web Search. In *SIGIR '21: The 44th International ACM SIGIR Conference on Research and Development in Information Retrieval, Virtual Event, Canada, July 11–15, 2021*, Fernando Diaz, Chirag Shah, Torsten Suel, Pablo Castells, Rosie Jones, and Tetsuya Sakai (Eds.). ACM, 1259–1268. doi:10.1145/3404835.3462895
- [28] Meng Liu, Zhengyang Wang, and Shuiwang Ji. 2022. Non-Local Graph Neural Networks. *IEEE Trans. Pattern Anal. Mach. Intell.* 44, 12 (2022), 10270–10276. doi:10.1109/TPAMI.2021.3134200
- [29] Sitao Luan, Chenqing Hua, Qincheng Lu, Jiaqi Zhu, Mingde Zhao, Shuyuan Zhang, Xiao-Wen Chang, and Doina Precup. 2022. Revisiting Heterophily For Graph Neural Networks. In *NeurIPS*.

- [30] Tuan Nguyen, Hirotada Honda, Takashi Sano, Vinh Nguyen, Shugo Nakamura, and Tan Minh Nguyen. 2024. From Coupled Oscillators to Graph Neural Networks: Reducing Over-smoothing via a Kuramoto Model-based Approach. In *International Conference on Artificial Intelligence and Statistics, 2-4 May 2024, Palau de Congressos, Valencia, Spain (Proceedings of Machine Learning Research, Vol. 238)*, Sanjoy Dasgupta, Stephan Mandt, and Yingzhen Li (Eds.). PMLR, 2710–2718. <https://proceedings.mlr.press/v238/nguyen24c.html>
- [31] Hongbin Pei, Bingzhe Wei, Kevin Chen-Chuan Chang, Yu Lei, and Bo Yang. 2020. Geom-GCN: Geometric Graph Convolutional Networks. In *8th International Conference on Learning Representations, ICLR 2020, Addis Ababa, Ethiopia, April 26-30, 2020*. OpenReview.net.
- [32] Michael Poli, Stefano Massaroli, Junyoung Park, Atsushi Yamashita, Hajime Asama, and Jinkyoo Park. 2019. Graph Neural Ordinary Differential Equations. *CoRR* abs/1911.07532 (2019). arXiv:1911.07532 <http://arxiv.org/abs/1911.07532>
- [33] Benedek Rozemberczki, Carl Allen, and Rik Sarkar. 2019. Multi-scale Attributed Node Embedding. *CoRR* abs/1909.13021 (2019). arXiv:1909.13021
- [34] Benedek Rozemberczki and Rik Sarkar. 2020. Characteristic Functions on Graphs: Birds of a Feather, from Statistical Descriptors to Parametric Models. In *CIKM '20: The 29th ACM International Conference on Information and Knowledge Management, Virtual Event, Ireland, October 19-23, 2020*. ACM. doi:10.1145/3340531.3411866
- [35] Benedek Rozemberczki and Rik Sarkar. 2020. Characteristic Functions on Graphs: Birds of a Feather, from Statistical Descriptors to Parametric Models. In *CIKM '20: The 29th ACM International Conference on Information and Knowledge Management, Virtual Event, Ireland, October 19-23, 2020*. ACM. doi:10.1145/3340531.3411866
- [36] T. Konstantin Rusch, Ben Chamberlain, James Rowbottom, Siddhartha Mishra, and Michael M. Bronstein. 2022. Graph-Coupled Oscillator Networks. In *International Conference on Machine Learning, ICML 2022, 17-23 July 2022, Baltimore, Maryland, USA (Proceedings of Machine Learning Research, Vol. 162)*, Kamalika Chaudhuri, Stefanie Jegelka, Le Song, Csaba Szepesvári, Gang Niu, and Sivan Sabato (Eds.). PMLR, 18888–18909. <https://proceedings.mlr.press/v162/rusch22a.html>
- [37] Oleksandr Shchur, Maximilian Mumme, Aleksandar Bojchevski, and Stephan Günnemann. 2018. Pitfalls of Graph Neural Network Evaluation. *CoRR* abs/1811.05868 (2018). arXiv:1811.05868
- [38] Jonathan Shlomi, Peter W. Battaglia, and Jean-Roch Vlimant. 2021. Graph neural networks in particle physics. *Mach. Learn. Sci. Technol.* 2, 2 (2021), 21001. doi:10.1088/2632-2153/ABBF9A
- [39] David I. Shuman, Sunil K. Narang, Pascal Frossard, Antonio Ortega, and Pierre Vandergheynst. 2013. The Emerging Field of Signal Processing on Graphs: Extending High-Dimensional Data Analysis to Networks and Other Irregular Domains. *IEEE Signal Process. Mag.* 30, 3 (2013), 83–98. doi:10.1109/MSP.2012.2235192
- [40] Yunchong Song, Chenghu Zhou, Xinbing Wang, and Zhouhan Lin. 2023. Ordered GNN: Ordering Message Passing to Deal with Heterophily and Over-smoothing. In *The Eleventh International Conference on Learning Representations, ICLR 2023, Kigali, Rwanda, May 1-5, 2023*. OpenReview.net. <https://openreview.net/pdf?id=wKPmPBHSnT6>
- [41] Susheel Suresh, Vinith Budde, Jennifer Neville, Pan Li, and Jianzhu Ma. 2021. Breaking the Limit of Graph Neural Networks by Improving the Assortativity of Graphs with Local Mixing Patterns. In *KDD '21: The 27th ACM SIGKDD Conference on Knowledge Discovery and Data Mining, Virtual Event, Singapore, August 14-18, 2021*, Feida Zhu, Beng Chin Ooi, and Chunyan Miao (Eds.). ACM, 1541–1551. doi:10.1145/3447548.3467373
- [42] Matthew Thorpe, Tan Minh Nguyen, Hedi Xia, Thomas Strohmer, Andrea L. Bertozzi, Stanley J. Osher, and Bao Wang. 2022. GRAND++: Graph Neural Diffusion with A Source Term. In *The Tenth International Conference on Learning Representations, ICLR 2022, Virtual Event, April 25-29, 2022*. OpenReview.net. <https://openreview.net/forum?id=EMxu-dzvjK>
- [43] Petar Velickovic, Guillem Cucurull, Arantxa Casanova, Adriana Romero, Pietro Lió, and Yoshua Bengio. 2018. Graph Attention Networks. In *6th International Conference on Learning Representations, ICLR 2018, Vancouver, BC, Canada, April 30 - May 3, 2018, Conference Track Proceedings*. OpenReview.net.
- [44] Xiyuan Wang and Muhan Zhang. 2022. How Powerful are Spectral Graph Neural Networks. In *International Conference on Machine Learning, ICML 2022, 17-23 July 2022, Baltimore, Maryland, USA (Proceedings of Machine Learning Research, Vol. 162)*, Kamalika Chaudhuri, Stefanie Jegelka, Le Song, Csaba Szepesvári, Gang Niu, and Sivan Sabato (Eds.). PMLR, 23341–23362. <https://proceedings.mlr.press/v162/wang22am.html>
- [45] Yifei Wang, Yisen Wang, Jiansheng Yang, and Zhouchen Lin. 2021. Dissecting the Diffusion Process in Linear Graph Convolutional Networks. In *Advances in Neural Information Processing Systems 34: Annual Conference on Neural Information Processing Systems 2021, NeurIPS 2021, December 6-14, 2021, virtual*, Marc Aurelio Ranzato, Alina Beygelzimer, Yann N. Dauphin, Percy Liang, and Jennifer Wortman Vaughan (Eds.). 5758–5769. <https://proceedings.neurips.cc/paper/2021/hash/2d95666e2649f6c63af75e09f5adb9-Abstract.html>
- [46] Felix Wu, Amauri H. Souza Jr., Tianyi Zhang, Christopher Fifty, Tao Yu, and Kilian Q. Weinberger. 2019. Simplifying Graph Convolutional Networks. In *Proceedings of the 36th International Conference on Machine Learning, ICML 2019, 9-15 June 2019, Long Beach, California, USA*. PMLR.
- [47] Shuwen Wu, Fei Sun, Wentao Zhang, Xu Xie, and Bin Cui. 2023. Graph Neural Networks in Recommender Systems: A Survey. *ACM Comput. Surv.* 55, 5 (2023), 97:1–97:37. doi:10.1145/3535101
- [48] Zonghan Wu, Shirui Pan, Fengwen Chen, Guodong Long, Chengqi Zhang, and Philip S. Yu. 2021. A Comprehensive Survey on Graph Neural Networks. *IEEE Trans. Neural Networks Learn. Syst.* 32, 1 (2021), 4–24. doi:10.1109/TNNLS.2020.2978386
- [49] Louis-Pascal A. C. Xhonneux, Meng Qu, and Jian Tang. 2020. Continuous Graph Neural Networks. In *Proceedings of the 37th International Conference on Machine Learning, ICML 2020, 13-18 July 2020, Virtual Event (Proceedings of Machine Learning Research, Vol. 119)*. PMLR, 10432–10441. <http://proceedings.mlr.press/v119/xhonneux20a.html>
- [50] Keyulu Xu, Chengtao Li, Yonglong Tian, Tomohiro Sonobe, Ken-ichi Kawarabayashi, and Stefanie Jegelka. 2018. Representation Learning on Graphs with Jumping Knowledge Networks. In *Proceedings of the 35th International Conference on Machine Learning, ICML 2018, Stockholm, Sweden, July 10-15, 2018*. PMLR.
- [51] Yujun Yan, Milad Hashemi, Kevin Swersky, Yaoqing Yang, and Danai Koutra. 2022. Two Sides of the Same Coin: Heterophily and Oversmoothing in Graph Convolutional Neural Networks. In *IEEE International Conference on Data Mining, ICDM 2022, Orlando, FL, USA, November 28 - Dec. 1, 2022*. IEEE. doi:10.1109/ICDM54844.2022.00169
- [52] Zhilin Yang, William W. Cohen, and Ruslan Salakhutdinov. 2016. Revisiting Semi-Supervised Learning with Graph Embeddings. In *Proceedings of the 33rd International Conference on Machine Learning, ICML 2016, New York City, NY, USA, June 19-24, 2016*. JMLR.org.
- [53] Wentao Zhang, Zeang Sheng, Ziqi Yin, Yuezhian Jiang, Yikuan Xia, Jun Gao, Zhi Yang, and Bin Cui. 2022. Model Degradation Hinders Deep Graph Neural Networks. In *KDD '22: The 28th ACM SIGKDD Conference on Knowledge Discovery and Data Mining, Washington, DC, USA, August 14 - 18, 2022*, Aidong Zhang and Huzefa Rangwala (Eds.). ACM, 2493–2503. doi:10.1145/3534678.3539374
- [54] Jialin Zhao, Yuxiao Dong, Ming Ding, Evgeny Kharlamov, and Jie Tang. 2021. Adaptive Diffusion in Graph Neural Networks. In *Advances in Neural Information Processing Systems 34: Annual Conference on Neural Information Processing Systems 2021, NeurIPS 2021, December 6-14, 2021, virtual*, Marc Aurelio Ranzato, Alina Beygelzimer, Yann N. Dauphin, Percy Liang, and Jennifer Wortman Vaughan (Eds.). 23321–23333. <https://proceedings.neurips.cc/paper/2021/hash/c42af2fa7356818e0389593714f59b52-Abstract.html>
- [55] Xuebin Zheng, Bingxin Zhou, Junbin Gao, Yuguang Wang, Pietro Lió, Ming Li, and Guido Montúfar. 2021. How Framelets Enhance Graph Neural Networks. In *Proceedings of the 38th International Conference on Machine Learning, ICML 2021, 18-24 July 2021, Virtual Event (Proceedings of Machine Learning Research, Vol. 139)*, Marina Meila and Tong Zhang (Eds.). PMLR, 12761–12771. <http://proceedings.mlr.press/v139/zheng21c.html>
- [56] Jiong Zhu, Yujun Yan, Lingxiao Zhao, Mark Heimann, Leman Akoglu, and Danai Koutra. 2020. Beyond Homophily in Graph Neural Networks: Current Limitations and Effective Designs. In *Advances in Neural Information Processing Systems 33: Annual Conference on Neural Information Processing Systems 2020, NeurIPS 2020, December 6-12, 2020, virtual*.

A Detailed mathematical derivation

A.1 Proof of Proposition 1

PROOF. Since $\mathbf{L} = \mathbf{D} - \mathbf{A}$, then

$$\begin{aligned} \mathbf{L}\mathbf{X} &= (\mathbf{D} - \mathbf{A})\mathbf{X} \\ &= \left(\begin{bmatrix} \sum_j A_{1j} & \cdots & 0 \\ \vdots & \ddots & \vdots \\ 0 & \cdots & \sum_j A_{Nj} \end{bmatrix} - \begin{bmatrix} A_{11} & \cdots & A_{1N} \\ \vdots & \ddots & \vdots \\ A_{N1} & \cdots & A_{NN} \end{bmatrix} \right) \begin{bmatrix} \mathbf{x}_1 \\ \vdots \\ \mathbf{x}_N \end{bmatrix} \\ &= \begin{bmatrix} \sum_j A_{1j} - A_{11} & \cdots & -A_{1N} \\ \vdots & \ddots & \vdots \\ -A_{N1} & \cdots & \sum_j A_{Nj} - A_{NN} \end{bmatrix} \begin{bmatrix} \mathbf{x}_1 \\ \vdots \\ \mathbf{x}_N \end{bmatrix} \\ &= [\dots, \sum_{v_j \in \mathcal{N}(v_i)} (\mathbf{x}_i - \mathbf{x}_j), \dots]^\top. \end{aligned} \quad (19)$$

where $A_{ij} = 1$, if $e_{ij} \in \mathcal{E}$; $A_{ij} = 0$, otherwise. Hence, the graph wave equation can be rewritten as:

$$\frac{\partial^2 \mathbf{X}}{\partial t^2} = a^2 \mathbf{L}\mathbf{X}. \quad (20)$$

□

A.2 Derivation of Explicit Scheme

For any node v_i at time t , we first discretize t as $t_n = n\tau$ ($n = 0, 1, \dots$). Then, considering its node representation \mathbf{x}_i along with a time step τ , its time difference of wave equation is given by:

$$\frac{\partial^2 \mathbf{X}(\mathbf{x}_i, t_n)}{\partial t^2} = \sum_{v_j \in \mathcal{N}(v_i)} L_{ij}^{(n)} (\mathbf{x}_j^{(n)} - \mathbf{x}_i^{(n)}), \quad (21)$$

where $L_{ij}^{(n)}$ denotes the element of \mathbf{L}_a . Moreover, we can expand at point (\mathbf{x}_i, t_n) using Taylor series, and obtain

$$\begin{aligned} &\frac{\mathbf{X}(\mathbf{x}_i, t_{n+1}) - 2\mathbf{X}(\mathbf{x}_i, t_n) + \mathbf{X}(\mathbf{x}_i, t_{n-1}))}{\tau^2} \\ &= \frac{\partial^2 \mathbf{X}(\mathbf{x}_i, t_n)}{\partial t^2} + \frac{\tau^2}{12} \frac{\partial^4 \mathbf{X}(\mathbf{x}_i, t_n)}{\partial t^4} + O(\tau^4). \end{aligned} \quad (22)$$

By substituting Eq. (21) into Eq. (22), we obtain

$$\begin{aligned} &\frac{\mathbf{X}(\mathbf{x}_i, t_{n+1}) - 2\mathbf{X}(\mathbf{x}_i, t_n) + \mathbf{X}(\mathbf{x}_i, t_{n-1}))}{\tau^2} \\ &= \sum_{v_j \in \mathcal{N}(v_i)} L_{ij}^{(n)} (\mathbf{x}_j^{(n)} - \mathbf{x}_i^{(n)}) + R_i^{(n)}(\mathbf{X}), \end{aligned} \quad (23)$$

where $R_i^{(n)}(\mathbf{X}) = \frac{\tau^2}{12} \frac{\partial^4}{\partial t^4} \mathbf{X}(\mathbf{x}_i, t_n) + O(\tau^4)$ denotes the truncation error. By truncating it, we obtain the forward time difference

$$\frac{\mathbf{X}_i^{(n+1)} - 2\mathbf{X}_i^{(n)} + \mathbf{X}_i^{(n-1)}}{\tau^2} = \sum_{v_j \in \mathcal{N}(v_i)} L_{ij}^{(n)} (\mathbf{x}_j^{(n)} - \mathbf{x}_i^{(n)}), \quad (24)$$

where $\mathbf{X}_i^{(n)}$ ($n = 1, 2, \dots$) denotes the approximate value of \mathbf{X} at (\mathbf{x}_i, t_n) . Transforming the Eq. (24) into matrix form

$$\frac{\mathbf{X}^{(n+1)} - 2\mathbf{X}^{(n)} + \mathbf{X}^{(n-1)}}{\tau^2} = \mathbf{L}_a^{(n)} \mathbf{X}^{(n)}. \quad (25)$$

We define the problem of solving the partial differential equation as an initial value problem, with the initial values given by the

second-order central difference quotient:

$$\mathbf{X}^{(0)} = \varphi_0(\mathbf{X}), \quad (26)$$

$$\frac{\mathbf{X}^{(1)} - \mathbf{X}^{(-1)}}{2\tau} = \varphi_1(\mathbf{X}), \quad (27)$$

where $\varphi_1(\mathbf{X})$ and $\varphi_2(\mathbf{X})$ can be obtained through neural layers. Let $n = 0$, then

$$\frac{\mathbf{X}^{(1)} - 2\mathbf{X}^{(0)} + \mathbf{X}^{(-1)}}{\tau^2} = \mathbf{L}_a^{(0)} \mathbf{X}^{(0)}. \quad (28)$$

By eliminating $\mathbf{X}^{(-1)}$ using the initial value Eq. (27), we obtain the node representation at time t_1 :

$$\mathbf{X}^{(1)} = \tau\varphi_1(\mathbf{X}) + \left(\mathbf{I} + \frac{\tau^2}{2} \mathbf{L}_a^{(0)} \right) \varphi_0(\mathbf{X}). \quad (29)$$

Finally, we can derive the node representation at time t_{n+1} :

$$\mathbf{X}^{(n+1)} = \left(2\mathbf{I} + \tau^2 \mathbf{L}_a^{(n)} \right) \mathbf{X}^{(n)} - \mathbf{X}^{(n-1)}. \quad (30)$$

A.3 Proof of Theorem 2

According to **Theorem 1**, to prove the stability of the explicit scheme $\mathbf{X}^{(n+1)} = \mathbf{A}\mathbf{X}^{(n)}$, we would like to prove that $|\lambda|_{max} \leq 1$.

PROOF. To facilitate the stability analysis of the explicit scheme $\mathbf{X}^{(n+1)} = (2\mathbf{I} + \tau^2 \mathbf{L}_a) \mathbf{X}^{(n)} - \mathbf{X}^{(n-1)}$, we first need to transform it into the form of $\mathbf{U}^{(n+1)} = \mathbf{C}\mathbf{U}^{(n)}$. Therefore, we assume

$$\mathbf{U}^{(n+1)} = \begin{bmatrix} \mathbf{X}^{(n+1)} \\ \mathbf{X}^{(n)} \end{bmatrix}, \mathbf{C} = \begin{bmatrix} \mathbf{C}_1 & \mathbf{C}_2 \\ \mathbf{C}_3 & \mathbf{C}_4 \end{bmatrix}, \quad (31)$$

then, we can obtain the system of linear equations:

$$\begin{cases} \mathbf{X}^{(n+1)} = \mathbf{C}_1 \mathbf{X}^{(n)} + \mathbf{C}_2 \mathbf{X}^{(n-1)} \\ \mathbf{X}^{(n)} = \mathbf{C}_3 \mathbf{X}^{(n)} + \mathbf{C}_4 \mathbf{X}^{(n-1)} \end{cases}. \quad (32)$$

According the equation of the explicit scheme, we can obtain the values of each block matrix in \mathbf{C} :

$$\mathbf{C}_1 = 2\mathbf{I} + \tau^2 \mathbf{L}_a, \mathbf{C}_2 = -\mathbf{I}, \mathbf{C}_3 = \mathbf{I}, \mathbf{C}_4 = \mathbf{0}, \quad (33)$$

resulting in $\mathbf{C}^{(n)}$ as follows:

$$\mathbf{C} = \begin{bmatrix} 2\mathbf{I} + \tau^2 \mathbf{L}_a & -\mathbf{I} \\ \mathbf{I} & \mathbf{0} \end{bmatrix}. \quad (34)$$

According to the **Theorem 1**, now we only need to compute the spectral radius of matrix \mathbf{C} to determine the condition that ensures the stability of the explicit scheme.

For convenience, we still use \mathbf{C}_1 instead of $2\mathbf{I} + \tau^2 \mathbf{L}_a$, and let λ, λ' denote the eigenvalue of \mathbf{C}, \mathbf{C}_1 , respectively. Then, the characteristic determinant of \mathbf{C} is given by:

$$\begin{aligned} \det\{\mathbf{C} - \lambda \mathbf{I}_{2N}\} &= \begin{vmatrix} \mathbf{C}_1 - \lambda \mathbf{I} & -\mathbf{I} \\ \mathbf{I} & -\lambda \mathbf{I} \end{vmatrix} = \left| (1 + \lambda^2) \mathbf{I} - \lambda \mathbf{C}_1 \right| \\ &= \left| \frac{1 + \lambda^2}{\lambda} \mathbf{I} - \mathbf{C}_1 \right| = 0. \end{aligned} \quad (35)$$

Evidently, $\left| \frac{1 + \lambda^2}{\lambda} \mathbf{I} - \mathbf{C}_1 \right| = 0$ is the characteristic equation of \mathbf{C}_1 , with the eigenvalue $\lambda' = \frac{1 + \lambda^2}{\lambda}$. According to the \mathbf{L}_a 's eigenvalue belongs to the interval $[-1, 1]$, then $\lambda' \in [2 - \tau^2, 2 + \tau^2]$. Next, we will investigate the range of values for λ .

Considering the equation obtained from $\lambda' = \frac{1 + \lambda^2}{\lambda}$:

$$\lambda^2 - \lambda' \lambda + 1 = 0, \lambda' \in [2 - \tau^2, 2 + \tau^2]. \quad (36)$$

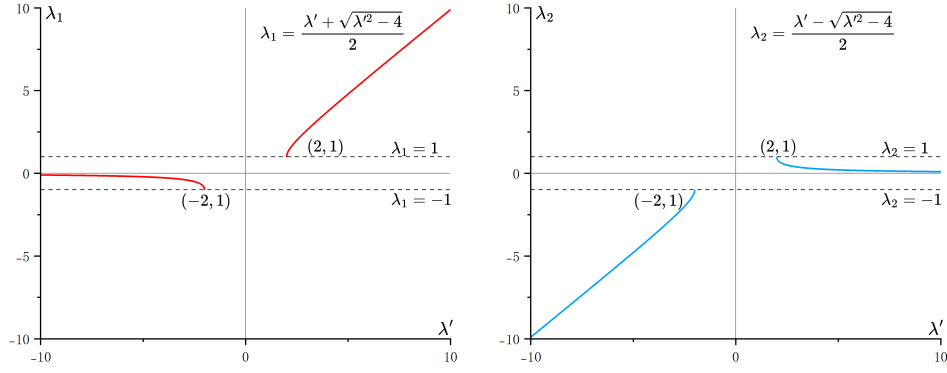


Figure 7: The function curve of real roots λ_1 (Left) and λ_2 (Right).

If $\Delta = \lambda'^2 - 4 < 0$, that is $-2 < \lambda' < 2$, then the equation has a pair of complex conjugate roots $\lambda_1 = \frac{\lambda' + i\sqrt{4 - \lambda'^2}}{2}$ and $\lambda_2 = \frac{\lambda' - i\sqrt{4 - \lambda'^2}}{2}$. And if $\Delta = \lambda'^2 - 4 \geq 0$, that is $|\lambda'| \geq 2$, then the equation has a pair of real roots $\lambda_1 = \frac{\lambda' + \sqrt{\lambda'^2 - 4}}{2}$ and $\lambda_2 = \frac{\lambda' - \sqrt{\lambda'^2 - 4}}{2}$. We next discuss whether the $|\lambda| \leq 1$ satisfies for different τ , considering different cases.

Case 1. If $\tau \in (0, 2)$.

a) When $\lambda' \in [2 - \tau^2, 2)$, the equation has a pair of complex conjugate roots $\lambda_{1,2}$. Evidently, $|\lambda_{1,2}| = \sqrt{\left(\frac{\lambda'}{2}\right)^2 + \left(\frac{\sqrt{4 - \lambda'^2}}{2}\right)^2} = 1$. Therefore, for any $\tau \in (0, 2)$, $|\lambda_{1,2}| \leq 1$.

b) When $\lambda' \in [2, 2 + \tau^2]$, the equation has a pair of real roots $\lambda_{1,2}$.

As shown in Figure 7 (Left), when $\lambda' = 2$, $|\lambda_1| = 1$, τ can take any positive real number at $(0, 2)$.

As shown in Figure 7 (Right), when $\lambda' \geq 2$, $|\lambda_2| \leq 1$, τ can take any positive real number at $(0, 2)$.

Caes 2. If $\tau \in [2, +\infty)$.

a) When $\lambda' \in [2 - \tau^2, -2]$, the equation has a pair of real roots $\lambda_{1,2}$.

As shown in Figure 7 (Left), when $\lambda' \leq -2$, $|\lambda_1| \leq 1$, τ can take any positive real number at $[2, +\infty)$.

As shown in Figure 7 (Right), when $\lambda' = -2$, $|\lambda_2| = 1$, τ can take any positive real number at $[2, +\infty)$.

b) When $\lambda' \in (-2, 2)$, the equation has a pair of complex conjugate roots $\lambda_{1,2}$. Evidently, $|\lambda_{1,2}| = 1$. Therefore, for any $\tau \in [2, +\infty)$, $|\lambda_{1,2}| \leq 1$.

c) When $\lambda' \in [2, 2 + \tau^2]$, the equation has a pair of real roots $\lambda_{1,2}$.

As shown in Figure 7 (Left), when $\lambda' = 2$, $|\lambda_1| = 1$, τ can take any positive real number at $[2, +\infty)$.

As shown in Figure 7 (Right), when $\lambda' \geq 2$, $|\lambda_2| \leq 1$, τ can take any positive real number at $[2, +\infty)$.

In conclusion, when $\tau \in \mathbb{R}^+$, the eigenvalues λ of \mathbf{C} satisfy $|\lambda| \leq 1$, then the explicit scheme based on symmetric normalized Laplacian is constantly stable. \square

A.4 Derivation of GWN-fa

Given frequency adaptive Laplacian as follow:

$$\mathbf{L}_{a,l}^{(n)} = \varepsilon^{(n)} \mathbf{I} + \mathbf{D}^{-\frac{1}{2}} \mathbf{A} \mathbf{D}^{-\frac{1}{2}}, \quad \mathbf{L}_{a,h}^{(n)} = \varepsilon^{(n)} \mathbf{I} - \mathbf{D}^{-\frac{1}{2}} \mathbf{A} \mathbf{D}^{-\frac{1}{2}}, \quad (37)$$

where $\mathbf{L}_{a,l}^{(n)}$ is a low-pass filter, and $\mathbf{L}_{a,h}^{(n)}$ is a high-pass filter. Based on the aforementioned two Laplacian, we can capture the low-frequency and high-frequency signals at time t_{n+1} :

$$\begin{aligned} \mathbf{X}_l^{(n+1)} &= \left(2\mathbf{I} + \tau^2 \left(\varepsilon^{(n)} \mathbf{I} + \mathbf{D}^{-\frac{1}{2}} \mathbf{A} \mathbf{D}^{-\frac{1}{2}} \right) \right) \mathbf{X}^{(n)} - \mathbf{X}^{(n-1)}, \\ \mathbf{X}_h^{(n+1)} &= \left(2\mathbf{I} + \tau^2 \left(\varepsilon^{(n)} \mathbf{I} - \mathbf{D}^{-\frac{1}{2}} \mathbf{A} \mathbf{D}^{-\frac{1}{2}} \right) \right) \mathbf{X}^{(n)} - \mathbf{X}^{(n-1)}. \end{aligned} \quad (38)$$

Then, we adaptively combine low-frequency and high-frequency signals using attention weights and obtain the feature vector of node v_i at time t_{n+1} :

$$\begin{aligned} \mathbf{x}_i^{(n+1)} &= \alpha_{l,ij}^{(n)} \mathbf{x}_{l,i}^{(n+1)} + \alpha_{h,ij}^{(n)} \mathbf{x}_{h,i}^{(n+1)} \\ &= \left(2 + \varepsilon^{(n)} \tau^2 \right) \alpha_{l,ij}^{(n)} \mathbf{x}_i^{(n)} + \sum_{v_j \in \mathcal{N}(v_i)} \frac{\tau^2 \alpha_{l,ij}^{(n)}}{\sqrt{\deg(v_i) \deg(v_j)}} \mathbf{x}_j^{(n)} - \alpha_{l,ij}^{(n)} \mathbf{x}_i^{(n-1)} \\ &\quad + \left(2 + \varepsilon^{(n)} \tau^2 \right) \alpha_{h,ij}^{(n)} \mathbf{x}_i^{(n)} - \sum_{v_j \in \mathcal{N}(v_i)} \frac{\tau^2 \alpha_{h,ij}^{(n)}}{\sqrt{\deg(v_i) \deg(v_j)}} \mathbf{x}_j^{(n)} - \alpha_{h,ij}^{(n)} \mathbf{x}_i^{(n-1)}, \end{aligned} \quad (39)$$

where $\deg(v)$ denotes the degree of node v . Let $\alpha_{ij}^{(n)} = \alpha_{l,ij}^{(n)} - \alpha_{h,ij}^{(n)}$ and $\alpha_{l,ij}^{(n)} + \alpha_{h,ij}^{(n)} = 1$, we have

$$\begin{aligned} \mathbf{x}_i^{(n+1)} &= \varepsilon^{(n)} \tau^2 \mathbf{x}_i^{(n)} \\ &\quad + \left(2\mathbf{x}_i^{(n)} + \sum_{v_j \in \mathcal{N}(v_i)} \frac{\tau^2 \alpha_{ij}^{(n)}}{\sqrt{\deg(v_i) \deg(v_j)}} \mathbf{x}_j^{(n)} \right) - \mathbf{x}_i^{(n-1)}. \end{aligned} \quad (40)$$

Weight $\alpha_{ij}^{(n)} = \tanh(\mathbf{g}^\top [\mathbf{x}_i^{(n)} || \mathbf{x}_j^{(n)}]) \in [-1, 1]$ can denote the correlation between nodes v_i and v_j , and it is computed using attention mechanism, where $\mathbf{g} \in \mathbb{R}^{2d}$ is a learnable parameter vector. Since ε is a learnable parameter, we can simplify $\varepsilon^{(n)} \tau^2$ as $\varepsilon^{(n)}$. Furthermore, in order to preserve the original node features, we replace $\mathbf{x}_i^{(n)}$ with $\mathbf{x}_i^{(0)}$ [3]. So we can obtain

$$\mathbf{x}_i^{(n+1)} = \varepsilon^{(n)} \mathbf{x}_i^{(0)} + \left(2\mathbf{x}_i^{(n)} + \sum_{v_j \in \mathcal{N}(v_i)} \frac{\tau^2 \alpha_{ij}^{(n)}}{\sqrt{\deg(v_i) \deg(v_j)}} \mathbf{x}_j^{(n)} \right) - \mathbf{x}_i^{(n-1)}. \quad (41)$$

Rewrite Eq. (41) in matrix form

$$\mathbf{X}^{(n+1)} = \varepsilon^{(n)} \mathbf{X}^{(0)} + \left(2\mathbf{I} + \tau^2 \boldsymbol{\alpha}^{(n)} \odot \mathbf{D}^{-\frac{1}{2}} \mathbf{A} \mathbf{D}^{-\frac{1}{2}}\right) \mathbf{X}^{(n)} - \mathbf{X}^{(n-1)}, \quad (42)$$

where the $\alpha_{ij}^{(n)}$ is the element of $\boldsymbol{\alpha}^{(n)}$.

A.5 Proof of Theorem 3

Similar to the proof of **Theorem 2** (in A.3), we prove the stability of frequency adaptive Laplacian.

PROOF. Given $\mathbf{L}_a = \mathbf{D}^{-\frac{1}{2}} \mathbf{A} \mathbf{D}^{-\frac{1}{2}}$, we have

$$\mathbf{L}_a = \varepsilon \mathbf{I} \pm \mathbf{D}^{-\frac{1}{2}} \mathbf{A} \mathbf{D}^{-\frac{1}{2}} = \varepsilon \mathbf{I} \pm \mathbf{L}_a, \quad (43)$$

and its eigenvalues satisfy $[\varepsilon - 1, \varepsilon + 1]$, $\varepsilon \in (0, 1)$.

According to the proof of **Theorem 1**, when \mathbf{L}_a 's eigenvalue belongs to the interval $[\varepsilon - 1, \varepsilon + 1]$, then the eigenvalue λ' of $\mathbf{C}_1 = 2\mathbf{I} + \tau^2 \mathbf{L}_a$ satisfies $\lambda' \in [2 + \tau^2(\varepsilon - 1), 2 + \tau^2(\varepsilon + 1)]$. Next, we will investigate the range of values for λ .

Considering the equation obtained from $\lambda' = \frac{1+\lambda^2}{\lambda}$:

$$\lambda^2 - \lambda' \lambda + 1 = 0, \lambda' \in [2 + \tau^2(\varepsilon - 1), 2 + \tau^2(\varepsilon + 1)]. \quad (44)$$

If $\lambda'^2 - 4 < 0$, that is $-2 < \lambda' < 2$, then the equation has a pair of complex conjugate roots $\lambda_1 = \frac{\lambda' + i\sqrt{4-\lambda'^2}}{2}$ and $\lambda_2 = \frac{\lambda' - i\sqrt{4-\lambda'^2}}{2}$. And if $\lambda'^2 - 4 \geq 0$, that is $|\lambda'| \geq 2$, then the equation has real roots $\lambda_1 = \frac{\lambda' + \sqrt{\lambda'^2 - 4}}{2}$ and $\lambda_2 = \frac{\lambda' - \sqrt{\lambda'^2 - 4}}{2}$. We next discuss whether the $|\lambda| \leq 1$ satisfies for different τ , considering different cases.

Case 1. If $\tau \in \left(0, \frac{2}{\sqrt{1-\varepsilon}}\right)$.

a) When $\lambda' \in [2 + \tau^2(\varepsilon - 1), 2)$, the equation has a pair of complex conjugate roots $\lambda_{1,2}$. Evidently, $|\lambda_{1,2}| = 1$. Therefore, for any $\tau \in \left(0, \frac{2}{\sqrt{1-\varepsilon}}\right)$, $|\lambda_{1,2}| \leq 1$.

b) When $\lambda' \in [2, 2 + \tau^2(\varepsilon + 1)]$, the equation has a pair of real roots $\lambda_{1,2}$.

As shown in Figure 7 (Left), when $\lambda' = 2$, $|\lambda_1| = 1$, τ can take any positive real number at $\left(0, \frac{2}{\sqrt{1-\varepsilon}}\right)$.

As shown in Figure 7 (Right), when $\lambda' \geq 2$, $|\lambda_2| \leq 1$, τ can take any positive real number at $\left(0, \frac{2}{\sqrt{1-\varepsilon}}\right)$.

Case 2. If $\tau \in \left[\frac{2}{\sqrt{1-\varepsilon}}, +\infty\right)$.

a) When $\lambda' \in [2 + \tau^2(\varepsilon - 1), -2]$, the equation has a pair of real roots $\lambda_{1,2}$.

As shown in Figure 7 (Left), when $\lambda' \leq -2$, $|\lambda_1| \leq 1$, τ can take any positive real number at $\left[\frac{2}{\sqrt{1-\varepsilon}}, +\infty\right)$.

As shown in Figure 7 (Right), when $\lambda' = -2$, $|\lambda_2| = 1$, τ can take any positive real number at $\left[\frac{2}{\sqrt{1-\varepsilon}}, +\infty\right)$.

b) When $\lambda' \in (-2, 2)$, the equation has a pair of complex conjugate roots $\lambda_{1,2}$. Evidently, $|\lambda_{1,2}| = 1$. Therefore, for any $\tau \in \left[\frac{2}{\sqrt{1-\varepsilon}}, +\infty\right)$, $|\lambda_{1,2}| \leq 1$.

c) When $\lambda' \in [2, 2 + \tau^2(\varepsilon + 1)]$, the equation has a pair of real roots $\lambda_{1,2}$.

As shown in Figure 7 (Left), when $\lambda' = 2$, $|\lambda_1| = 1$, τ can take any positive real number at $\left[\frac{2}{\sqrt{1-\varepsilon}}, +\infty\right)$.

As shown in Figure 7 (Right), when $\lambda' \geq 2$, $|\lambda_2| \leq 1$, τ can take any positive real number at $\left[\frac{2}{\sqrt{1-\varepsilon}}, +\infty\right)$.

In conclusion, when $\tau \in R^+$, the eigenvalues λ of \mathbf{C} satisfy $|\lambda| \leq 1$, then the explicit scheme based on frequency adaptive Laplacian is constantly stable. \square

B Implementation Details

For all experiments, each method was run on a single NVIDIA Tesla V100 GPU with 16GB memory, and the CPU used is Intel Xeon E5-2660 v4 CPUs. All models train 200 epochs and employed an early stopping strategy triggered when the loss exceed the average loss of the last 10 epochs.

B.1 Dataset Statistics

Table 5 report the statistical information of datasets used in this paper.

Table 5: Dataset statistics.

Datasets	#Nodes	#Edges	#Features	#Classes
Cora	2708	5278	1433	7
CiteSeer	3327	4552	3703	6
PubMed	19717	44324	500	3
Computers	13752	245861	767	10
Photo	7650	119081	745	8
CS	18333	81894	6805	15
Actor	7600	30019	932	5
Texas	183	325	1703	5
Cornell	183	298	1703	5
Wisconsin	251	515	1703	5
DeezerEurope	28281	92752	128	2
ogbn-arxiv	169343	1166243	128	40

B.2 Parameter Search

We employ the wandb library for parameter search with Bayes scheme. The ranges for each hyperparameter are outlined in Table 6.

Table 6: The range of hyperparameters.

Parameters	Range	Distribution
Dimension d	{32, 64, 128, 256}	set
Time size τ	{0.2, 0.5, 1.0, 2.0, 5.0}	set
Terminal time T	[1, 20]	uniform
Dropout	[0, 0.8]	uniform
Learning rate	[0.001, 0.25]	log_uniform_values
Weight decay	[0, 0.1]	uniform

C Performance and Efficiency Analysis

We analyze the efficiency of GWN in Figure 8. We compare GWN at different τ with four basic GNNs and three variants of GRAND (GRAND-l, GRAND-nl, and GRAND-nl-rw). GWN-sym is faster than GWN-fa because it has fewer learnable parameters. And as τ increases, their runtime becomes faster. Taking CiteSeer as an example, "sym-1.0 (1.7x)" achieves both optimal performance and

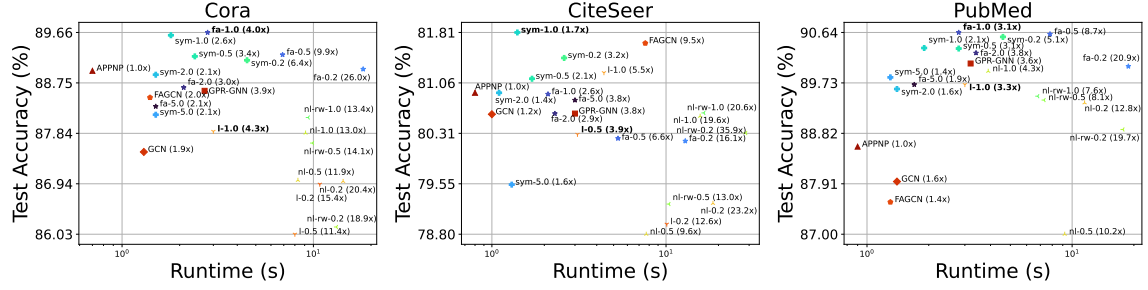


Figure 8: Accuracy and runtime of the methods: "sym" and "fa" denote two variants of GWN; "l", "nl", and "nl-rw" denote three variants of GRAND; "-1.0" denotes $\tau = 1.0$; (2.0x) denotes the multiple of the shortest runtime.

Table 7: The performances (%) and runtimes (s) of methods on homophilic datasets: mean accuracy \pm standard deviation on 60%/20%/20% random splits and 10 runs. sym-0.2 indicates GWN-sym under $\tau = 0.2$. Bold and underline indicate optimal and suboptimal results, respectively. OOM denotes out of memory.

Datasets	Cora	CiteSeer	PubMed	Computers	Photo	CS
SGC	86.10 \pm 1.37 (0.7)	80.35 \pm 1.33 (0.7)	83.45 \pm 0.51 (0.8)	84.45 \pm 0.56 (0.7)	88.95 \pm 0.86 (0.6)	95.15 \pm 0.24 (0.7)
APPNP	88.97 \pm 0.88 (0.7)	80.91 \pm 1.43 (0.8)	88.58 \pm 0.56 (0.9)	86.73 \pm 0.74 (0.8)	93.74 \pm 0.57 (0.8)	95.58 \pm 0.20 (1.6)
GPR-GNN	88.61 \pm 1.28 (2.7)	80.60 \pm 1.27 (3.0)	90.08 \pm 0.70 (3.2)	88.55 \pm 0.90 (1.4)	94.61 \pm 0.68 (2.5)	96.26 \pm 0.27 (1.3)
GCN	87.51 \pm 1.38 (1.3)	80.59 \pm 1.12 (1.0)	87.95 \pm 0.83 (1.4)	86.09 \pm 0.61 (1.3)	93.04 \pm 0.53 (1.4)	95.14 \pm 0.25 (0.9)
FAGCN	88.49 \pm 1.18 (1.4)	81.65 \pm 0.96 (7.6)	87.58 \pm 1.15 (1.3)	87.32 \pm 0.51 (1.2)	93.41 \pm 0.76 (1.0)	95.79 \pm 0.26 (4.8)
sym-0.2	89.16 \pm 0.80 (4.5)	81.43 \pm 1.73 (2.6)	90.56 \pm 0.54 (4.6)	89.97 \pm 0.56 (8.8)	94.82 \pm 0.43 (4.1)	96.60 \pm 0.28 (3.6)
sym-0.5	89.23 \pm 0.69 (2.4)	81.12 \pm 1.77 (1.7)	90.35 \pm 1.08 (2.8)	89.92 \pm 0.72 (3.8)	94.96 \pm 0.69 (3.6)	96.51 \pm 0.29 (2.8)
sym-1.0	89.61 \pm 0.87 (1.8)	81.81 \pm 1.70 (1.4)	90.36 \pm 0.75 (1.9)	90.10 \pm 0.87 (3.7)	95.31 \pm 0.65 (4.0)	96.66 \pm 0.26 (3.2)
sym-2.0	88.90 \pm 1.38 (1.5)	80.91 \pm 1.05 (1.1)	89.62 \pm 0.64 (1.4)	89.75 \pm 1.10 (2.0)	94.84 \pm 0.59 (1.9)	96.52 \pm 0.32 (2.3)
sym-5.0	88.18 \pm 1.14 (1.5)	79.54 \pm 1.44 (1.4)	89.83 \pm 0.30 (1.3)	90.01 \pm 1.12 (2.9)	94.83 \pm 0.69 (1.4)	95.91 \pm 0.26 (3.1)
fa-0.2	89.00 \pm 1.30 (18.2)	80.19 \pm 1.09 (12.9)	90.03 \pm 0.81 (18.8)	OOM	OOM	OOM
fa-0.5	89.26 \pm 0.73 (6.9)	80.23 \pm 1.71 (5.3)	90.61 \pm 0.77 (7.8)	OOM	95.25 \pm 0.55 (6.9)	96.53 \pm 0.25 (5.5)
fa-1.0	89.66 \pm 1.29 (2.8)	80.89 \pm 1.51 (2.1)	90.64 \pm 0.73 (2.8)	90.62 \pm 0.61 (5.6)	95.61 \pm 0.53 (3.5)	96.67 \pm 0.26 (8.6)
fa-2.0	88.67 \pm 1.56 (2.1)	80.60 \pm 1.77 (2.3)	90.27 \pm 0.82 (3.4)	89.29 \pm 0.99 (5.9)	94.22 \pm 0.59 (1.7)	96.62 \pm 0.30 (2.5)
fa-5.0	88.33 \pm 1.26 (1.5)	80.80 \pm 0.70 (3.0)	89.70 \pm 0.74 (1.7)	89.22 \pm 0.98 (3.6)	94.56 \pm 0.75 (2.3)	96.62 \pm 0.21 (5.4)

competitive efficiency. Furthermore, GRAND exhibits overall less efficiency, with its three variants mainly cluster on the right side of figures, and their runtimes are on the order of 10^1 . Considering its most efficient variant "l-0.5 (3.9x)", its performance and runtime are still inferior to our variant "sym-1.0 (1.7x)". It demonstrates that *our models can achieve both efficient and effective performance.*

As shown in Table 7 and Table 8, we present the complete performance and efficiency of GWN at different τ . The results and runtimes for all models are obtained using the optimal parameters. It is important to note that the runtime, in addition to time step τ , can be affected by parameters such as the number of layers, learning rate, and hidden layer dimensions. Therefore, there are cases where the runtime increases for larger τ compared to smaller τ .

Table 8: The performances (%) and runtimes (s) of methods on heterophilic datasets: mean accuracy \pm standard deviation on random splits and 10 runs. sym-0.2 indicates GWN-sym under $\tau = 0.2$. Bold and underline indicate optimal and suboptimal results, respectively.

Datasets Splits	Texas		Cornell		Wisconsin	
	48/32/20(%)	60/20/20(%)	48/32/20(%)	60/20/20(%)	48/32/20(%)	60/20/20(%)
SGC	-	74.90 \pm 8.23 (0.6)	-	60.60 \pm 11.92 (0.6)	-	63.75 \pm 5.14 (0.8)
APPNP	-	81.64 \pm 3.17 (1.2)	-	73.40 \pm 4.62 (1.3)	-	71.50 \pm 5.92 (1.5)
GPR-GNN	-	91.89 \pm 4.08 (0.9)	-	85.91 \pm 4.60 (0.8)	-	93.84 \pm 3.16 (0.9)
GCN	-	79.33 \pm 4.47 (2.2)	-	69.53 \pm 11.79 (2.9)	-	63.94 \pm 4.93 (1.1)
FAGCN	-	85.57 \pm 4.75 (4.6)	-	86.38 \pm 5.33 (3.7)	-	84.88 \pm 9.19 (5.6)
sym-0.2	89.85 \pm 5.05 (2.3)	91.48 \pm 5.40 (2.6)	87.03 \pm 7.41 (2.2)	88.30 \pm 6.04 (2.7)	89.85 \pm 4.57 (2.2)	91.62 \pm 3.12 (2.5)
sym-0.5	87.84 \pm 3.18 (1.7)	90.33 \pm 6.30 (1.6)	85.95 \pm 4.73 (1.8)	87.23 \pm 4.70 (1.7)	88.53 \pm 3.72 (1.7)	91.12 \pm 2.67 (1.7)
sym-1.0	86.47 \pm 3.13 (1.4)	88.52 \pm 2.56 (1.4)	83.14 \pm 5.52 (1.4)	84.26 \pm 4.40 (1.4)	85.74 \pm 5.10 (1.4)	88.75 \pm 3.78 (1.5)
sym-2.0	89.41 \pm 3.23 (1.1)	91.64 \pm 3.74 (1.2)	88.11 \pm 3.17 (1.1)	89.57 \pm 3.54 (1.1)	90.88 \pm 4.43 (1.0)	93.38 \pm 3.18 (1.1)
sym-5.0	82.75 \pm 4.41 (1.1)	84.59 \pm 5.02 (1.2)	84.59 \pm 5.56 (1.1)	87.23 \pm 5.85 (1.1)	85.15 \pm 3.06 (1.2)	87.50 \pm 4.49 (1.2)
fa-0.2	92.94 \pm 4.45 (4.4)	93.28 \pm 3.41 (5.1)	90.00 \pm 3.83 (4.2)	90.85 \pm 3.02 (5.9)	93.82 \pm 3.24 (3.7)	94.25 \pm 2.65 (4.2)
fa-0.5	92.16 \pm 2.61 (2.1)	92.79 \pm 3.01 (2.4)	90.27 \pm 7.12 (2.1)	92.13 \pm 3.76 (2.0)	94.12 \pm 3.02 (2.0)	94.75 \pm 1.85 (2.1)
fa-1.0	91.57 \pm 4.24 (1.8)	92.46 \pm 3.30 (1.8)	88.38 \pm 6.12 (1.8)	89.57 \pm 4.65 (1.7)	93.82 \pm 3.24 (2.0)	94.63 \pm 1.77 (1.8)
fa-2.0	91.74 \pm 3.06 (1.4)	93.28 \pm 4.19 (1.4)	90.81 \pm 4.63 (1.4)	91.28 \pm 3.81 (1.7)	94.26 \pm 1.76 (1.3)	95.63 \pm 1.59 (1.3)
fa-5.0	90.59 \pm 3.56 (1.3)	90.33 \pm 3.97 (1.3)	88.65 \pm 3.56 (1.3)	89.79 \pm 6.17 (1.5)	94.12 \pm 1.70 (1.2)	94.13 \pm 2.13 (1.4)